MODELING COASTAL PATHOGEN POPULATIONS: ADVANCEMENTS IN PREDICTIVE MODELING OF *VIBRIO VULNIFICUS* IN A TROPICAL URBAN ESTUARY IN HONOLULU, HAWAI‘I

A THESIS SUBMITTED TO THE GRADUATE DIVISION OF THE UNIVERSITY OF HAWAI‘I AT MĀNOA IN PARTIAL FULFILLMENT OF THE REQUIREMENTS FOR THE DEGREE OF

MASTER OF SCIENCE
IN
OCEANOGRAPHY

AUGUST 2021

Jessica A. Bullington

Thesis Committee
Craig Nelson, Chairperson
Margaret McManus
Grieg Steward

This thesis is dedicated to my mother and grandmother
who lit a path for women in the fields of biology and chemistry.

I am forever inspired by their strength and passion.

ACKNOWLEDGEMENTS

There are many people who have encouraged and supported me through the process of earning this degree and preparation of this thesis. Foremost, I thank my partner, Devin Williams, who always has my back and shows up to my presentations, who challenges me to think deeper and facilitates intellectual discussions, and who has made significant personal sacrifices to support my career. I thank my best friend, diving buddy, and colleague, Rachel Liu, who has provided endless feedback on grant and fellowship applications. I thank my best friend, Jenna Hively, who provided emotional support and sanity checks throughout the challenges of earning this degree.

My fellow students were an incredible support network and catalyst for growth. I thank my officemates who became my closest friends throughout the trials and tribulations of graduate school and put up with my endless questions in courses; Petra Byl, Gabby Stedman, Andrés Salazar Estrada, Oscar Ramfelt, Kirsten Poff, and Krissy Remple. I thank my lab mates who provided technical support and feedback on the evolution of my thesis project and presentations; Krissy Remple, Wesley Sparagon, Shayle Matsuda, Rayna McClintock, Brenna Carroll, Nic Vanderzyl, and Hendrikje Jorissen. In particular, I thank Krissy Remple who selflessly assisted my professional growth on many fronts and stuck with me during the chaos of conferences. I am also indebted to my lab bench sisters, Abby Golder and Bri Ornelas, who made the long nights of processing samples a pleasure. Their care and dedication ensured high quality data and peace of mind. I thank Ashley Hi‘ilani Sanchez, Nicole Yamase, and Krissy Remple who challenged me to dig deeper into the social constructs and flaws of science.

I extend my gratitude to all of the oceanography department faculty and staff who guided me and believed in my success. In particular, I thank Margaret McManus whose poise and leadership have set an example for my goals as a scientist. I thank Grieg Steward for his enthusiasm as a teacher and for my project, Brian Glazer who remained confident in my leadership abilities in the field, and Anna Neuheimer who managed to provide timely and approachable advice on statistics from the other side of the world. I also thank Kristin Momohara, Mireya Inga, and Catalpa Kong who run the department. I would be lost and confused without their generous help.

Finally, I thank my thesis advisor, Craig Nelson. Craig has consistently been an outstanding, above-and-beyond advisor and mentor to me. He facilitated outside opportunities for my professional growth in addition to my funded research project. He was patient, empathetic, and always ready to stand up in my defense. He immediately respected and valued my opinions and created space for me to share them. From the first hurricane warnings in 2018 to the COVID-19 pandemic, he was genuinely concerned for my safety and mental health. He has shown me that you can be humble and kind and still be a successful scientist. For every piece of advice, every weekly meeting, every manuscript revision, every immediate response on slack, thank you, Craig.

ABSTRACT

Vibrio vulnificus is a deadly pathogenic bacterium found worldwide in estuarine habitats. Predicting the presence and abundance of *V. vulnificus* is becoming more critical as sea level rises into densely populated urban areas and increasing water temperatures accelerate growth rates and expand habitat range. I explored two methods of modeling microbial populations, (1) statistical correlation with environmental covariates and (2) numerical modeling of growth and mortality rates, in order to improve predictive modeling capabilities of *V. vulnificus* in the Ala Wai Canal in Honolulu, Hawai‘i.

Chapter one of this thesis details research testing the hypothesis that incorporating measurements of dissolved organic and inorganic nutrients will improve the predictive power of statistical and forecasting models of *V. vulnificus*. In this field-based study, I parameterized linear regression models of *V. vulnificus* abundance using physical, optical, and chemical water properties in high spatial and temporal resolution to develop a real-time spatially-explicit model of *V. vulnificus* pathogen risk. A model including fine scale organic matter characterization and a small set of easily measured, highly significant environmental predictors could explain nearly 70% of variation in *V. vulnificus* abundance over an annual cycle. Using an oceanographic circulation model, I show how these models can be applied to predict plumes of *V. vulnificus* from the canal into the coastal environment. I also describe a framework for how continuous monitoring technology can be employed to nowcast and forecast the abundance of an aquatic pathogen. Long-term forecasts based on climate change projections estimate an overall increase in *V. vulnificus* density of up to 40 % by the end of the century due to increasing temperature. These novel findings will have significant ramifications to coastal pathogen monitoring programs and ongoing efforts to predict how climate change will alter the dynamics of estuarine microbial ecosystems.

Chapter two compares experimental approaches to calculate mortality rates of natural populations of *V. vulnificus* in order to improve an existing numerical population model of *V. vulnificus*. This model uses the environmental constraints of growth rates coupled to a physical circulation model, however, model predictions are inconsistent with field observations. Characterizing the environmental constraints of mortality rates would likely improve the model’s

accuracy and usefulness as a tool to communicate exposure risk. I tested the eukaryotic inhibition and dilution experiment techniques in order to quantify the contributions of grazing and viral lysis to natural mortality of the microbial community as a whole and *V. vulnificus*. My results show that eukaryotic inhibition may be a more effective technique to calculate mortality from predation than the dilution experiment technique. I outline several recommendations to improve the experimental design for interpretation and application. Ultimately, improving these predictive models of microbial populations is critical for management of waterborne pathogen risk exposure, particularly given the uncertainty of a changing global climate. This research represents a significant step forward to developing robust predictive modeling frameworks for coastal pathogens.

TABLE OF CONTENTS

LIST OF TABLES

LIST OF FIGURES

CHAPTER 1

Incorporating the spatiotemporal dynamics of dissolved nutrients and organic matter improves predictive models of *Vibrio vulnificus* concentrations in a tropical urban estuary

Keywords*: Vibrio vulnificus*, Pathogen, Estuary, Hawai‘i, Predictive Modeling, Climate Change, Nutrients, Dissolved Organic Matter, Groundwater

1.1 ABSTRACT

The south shore of O‘ahu, Hawai‘i is one of the most visited coastal tourism areas in the United States with some of the highest instances of recreational waterborne disease. The pathogenic bacterium, *Vibrio vulnificus*, lives in the warm temperature and intermediate salinity waters of the estuarine Ala Wai Canal in Honolulu which surrounds the heavily populated tourism center of Waikīkī. Heavy rainfall has been shown to transport water from the canal into the nearshore coastal system threatening human and ecological health as well as the state's tourism-based economy. I developed a biological-physical statistical model to predict *V. vulnificus* dynamics using environmental measurements that can be captured with moored oceanographic sensors in real time. I parameterized and validated the model using a novel approach that integrates data from three sources: 1) monthly profile measurements at each of 18 sites spanning an annual cycle which included *in situ* discrete sampling at 3 depths (surface, pycnocline, and bottom water) and continuous sensor profiling, 2) moored instrument continuous time series from the Pacific Islands Ocean Observing System (PacIOOS) and 3) the Waikīkī Regional Ocean Modeling System (ROMS). Discrete samples (n = 213) were analyzed for 36 biogeochemical variables and *V. vulnificus* density using quantitative PCR of the hemolysin A toxicity gene (*vvhA*). I found significant monthly variation in *V. vulnificus* density ranging over 4

orders of magnitude largely predictable by seasonality in biogeochemistry. The best multiple regression model of *V. vulnificus* concentration, explaining 70% of variation, included salinity, five-day average rainfall, daily maximum air temperature, silicate, dissolved oxygen and two metrics of dissolved organic matter fluorescence (visible humic-like fluorescent dissolved organic matter and the Humification Index). This result suggests a consistent response of *V. vulnificus* to freshwater inputs, particularly groundwater, and changes in organic matter resources. These linear models, paired with the PacIOOS time series and ROMS products, were then implemented to predict *V. vulnificus* density in the canal and coastal waters in real time across the nearshore Waikīkī region and were validated against measured values. Long-term climate model projections of local rainfall and air temperature were used to predict an overall increase in *V. vulnificus* density of approximately 20 to 40 % by 2100. Improving these predictive models of microbial populations is critical for management of waterborne pathogen risk exposure, particularly in the wake of a changing global climate.

1.2 INTRODUCTION

Vibrio vulnificus ***Biology and Vibriosis Infection***

Vibrio is a genus of Gram-negative heterotrophic bacteria with diverse life history strategies as free-living, host-associated, or particle-attached members of marine and estuarine microbial communities worldwide (Baker-Austin et al., 2018; Heng et al., 2017; Huang et al., 2016). Several *Vibrio* species are known human pathogens, including *V. cholerae*, *V. parahaemolyticus*, and *V. vulnificus*. Vibriosis infections occur through foodborne or recreational exposure with an annual healthcare cost to the U.S. nearing $300 million with approximately 85% of those costs attributed to *V. vulnificus* alone (Ralston et al., 2011). *V. vulnificus* is found in both free-living in brackish water and associated with sediment, algae, fish, molluscs, crustaceans, and zooplankton in warm estuarine environments globally (DePaola et al., 1994; Givens et al., 2014; Johnson et al., 2010; Maugeri et al., 2006; Turner et al., 2009). Although uncommon (approximately 100 cases are reported in the U.S. annually), the majority of *V. vulnificus* infections are from wound exposure to contaminated water, resulting in cellulitis and necrotizing fasciitis with a 25% case-fatality rate (Horseman & Surani, 2011). There is minimal monitoring for *V. vulnificus* in coastal waters worldwide (Baker-Austin et al., 2018), particularly at ecologically relevant scales that would allow for reliable forecasting of pathogen risk of exposure in contaminated waters. Prediction of the presence and abundance of *V. vulnificus* will become even more critical as sea level rises into populated areas and increasing water temperatures accelerate the pathogen's growth rate. Unlike many other aquatic human pathogens, *V. vulnificus* concentrations cannot be predicted effectively with fecal indicator bacteria because the pathogen lives naturally in estuarine habitats (Strom & Paranjpye, 2000).

The Estuarine Habitat of **Vibrio vulnificus**

Estuaries are heterogenous and idiosyncratic with unique biogeochemical features such as sharp gradients over short geographic areas and small depth ranges, high biological diversity and activity, and anoxic sediments (Cai, 2011). They are known to be effective traps for nutrients, sediments, and pollutants from inflowing rivers and runoff (Shiller, 1996). By nature of their proximity to populous areas, estuaries are at high risk of anthropogenic impact from

development and pollution. Due to complex and location-specific hydrology, oceanography, climatology, and human development, it is unknown how climate change will modify these environments, particularly estuarine microbial communities and the abundance of human pathogens (Ghosh & Bhadury, 2019; Kan et al., 2007).

Vibrio vulnificus ***Response to Climate Change***

There is empirical evidence for an increased abundance of *V. vulnificus* in bacterioplankton communities and infection rates over the past 50 years (Newton et al., 2012) which has been linked to increased sea surface temperature (Vezzulli et al., 2012; 2013; 2016). Additional climatological changes, such as increased frequency of hurricanes, storm surges, sea level rise, and coastal flooding, have been hypothesized to increase the geographic distribution of *V. vulnificus* and the incidence of *V. vulnificus* infections (Martinez-Urtaza et al., 2010; Muhling et al., 2017; Paz et al., 2007). Muhling et al. (2017) found significant increases in season length and spatial habitat for *V. vulnificus* in the Chesapeake Bay based on statistical downscaling of climate change projections. There is evidence for habitat expansion into higher latitudes (Baker-Austin et al., 2013; Paz et al., 2007) and a response of *V. vulnificus* to drought conditions (Wetz et al., 2013). Baker-Austin et al. (2017) even argue that *V. vulnificus*, given its response to temperature, be used as a barometer of climate change in marine environments. Despite these concerns, routine monitoring of natural *V. vulnificus* populations is infrequent in the U.S. Predictive models, based on the environmental conditions that govern *V. vulnificus* distribution and growth, may be a viable alternative to survey-based monitoring in order to provide an early warning of the risk of infection. Previous work by Jacobs et al. (2014) has shown promise at constructing such predictive spatially-explicit models. However, these efforts have been limited to probability of occurrence of *V. vulnificus* rather than absolute abundance which is more directly related to the risk of exposure.

Environmental Controls of **Vibrio vulnificus**

The environmental controls of *V. vulnificus* populations are poorly constrained aside from well-established effects of salinity and temperature on growth rates in laboratory cultures (Kaspar & Tamplin, 1993; Motes et al., 1998). Surveys and laboratory experiments have

documented that *V. vulnificus* is most prolific in water temperatures above 18 °C and salinity between 15 and 25 (Huehn et al., 2014; Jones & Oliver, 2009; Randa et al., 2004). There are several studies that assess the effects of additional parameters, such as turbidity, chlorophyll, nutrients and pH, on *V. vulnificus* growth and distribution (Lipp et al., 2001; O'Neill et al., 1992; Pfeffer et al., 2003; Tamplin et al., 1982; Wright et al., 1996). Fewer address the *in situ* environment with multiple interacting factors affecting growth and mortality. Environmental measurements of *V. vulnificus* density show strong seasonal dynamics where *V. vulnificus* density is higher in warm summer months in temperate and subtropical areas (Jacobs et al., 2014; Pfeffer et al., 2003; Tamplin et al., 1982). However, there is minimal data from tropical areas where water temperatures remain above 18 °C year-round and other environmental controls may be more important determinants of *V. vulnificus* density.

Previous work on* Vibrio vulnificus *in Hawai'i

In Hawai'i, recreational exposure to *Vibrio* contaminated water is likely high, and rates of *Vibrio* infections are reportedly five times higher than any other U.S. state per capita (National Center for Emerging & Infectious Diseases). *V. vulnificus* is found ubiquitously in the Ala Wai Canal, a prominent waterway in Honolulu, Hawai'i (Nigro, 2012). Previous surveys of the canal have shown that variability in *V. vulnificus* abundance scales with temporal resolution (Nigro, 2012). The range and variability of *V. vulnificus* abundance is smaller for shorter time scales (weekly, daily, hourly) than for monthly or seasonal patterns in abundance. Therefore, I focused my research in this study on capturing aspects of seasonal variation as important determinants of *V. vulnificus* variation. Preliminary work from 2008 – 2009 found significantly higher abundances of *V. vulnificus* in the canal during the rainy season from October – March (Nigro, 2012). In addition, Nigro (2012) found evidence to suggest a varied response of *V. vulnificus* to different freshwater sources with a salinity optimum of 12. There also appeared to be different dynamics between the infectious C-type strain and noninfectious E-type strain where the proportion of C-type increased with higher salinity values. However, the Nigro (2012) study was limited to surface sampling and a limited number of environmental measurements (salinity, temperature, chlorophyll-a, particulate carbon, phosphate, nitrate, nitrite, and ammonium) from bottle samples. These previous results hint at a response of *V. vulnificus* to freshwater flow and

nutrient resources that are useful for characterizing environmental controls but require further exploration for statistical and predictive modeling. Previous modeling attempts using a coupled physical circulation and numerical model of *V. vulnificus* growth rate in response to salinity and temperature by Nuss (2016) resulted in significant discrepancies between modeled and measured *V. vulnificus* abundance and patterns of variation in the canal. The addition of nutrient and organic matter resources into predictive models of *V. vulnificus* abundance may therefore improve predictive capabilities.

Project Objectives

In order to parameterize the distribution and abundance of this pathogen in the Ala Wai Canal and adjacent recreational coastal waters, I measured temporal and spatial variation in *V. vulnificus* over an annual cycle in concert with an array of biogeochemical parameters. Using these dynamic relationships, I built a spatially-explicit predictive model to assist mitigation efforts and limit the threat to human health. Past work has demonstrated that salinity and temperature variation alone do not sufficiently explain *V. vulnificus* population dynamics for predictive modeling, especially for this tropical location where water temperature is always in an optimal range. I hypothesized that model parameterization with measurements of nutrient and organic matter concentrations would improve model strength and capture significantly more seasonal and geographical variation in *V. vulnificus* density. I present a robust predictive model of *V. vulnificus* density based on comprehensive measurements of environmental variables at high-resolution ecologically-relevant spatial and temporal scales. Leveraging an existing coastal oceanographic time series and turbidity plume forecast model (Johnson et al., 2013) maintained by the Pacific Islands Ocean Observing System (PacIOOS), I applied the statistical model to construct a real time model of *V. vulnificus* density throughout nearshore Waikīkī in order to provide more timely information on pathogen risk assessment. In addition, I report a long-term forecast projection of *V. vulnificus* densities with climate change.

1.3 MATERIALS AND METHODS

The Ala Wai Canal Study Site

The Ala Wai Canal is a prominent waterway in urban Honolulu, Hawai‘i on the island of O‘ahu. The canal was constructed during the 1920s by the U.S. Army Corps of Engineers in order to drain the Waikīkī wetlands for coastal development. The canal is channelized with cement and extends for roughly 3 km parallel to the shoreline varying from 51 to 83 m wide with one major bend towards the ocean. Currently, the canal operates as a tidally-influenced estuary with freshwater input from the Makiki stream, Mānoa-Pālolo drainage, and several small urban runoff drains. The mouth of the canal is located at the Ala Wai Boat Harbor centered between the popular Waikīkī beaches to the east and Ala Moana Beach Park to the west. In this potential outflow area, there is high recreational activity, including surfing, paddling, sailing, swimming, and fishing. Therefore, there is a concerning risk of exposure to *V. vulnificus* in this area. The Clean Water Branch (CWB) of the Hawai‘i State Department of Health is responsible for the protection and monitoring of the coastal ecosystem in the state. The CWB tests coastal waters for fecal indicator bacteria concentrations (*Enterococcus spp.* and *Clostridium perfringens*), as well as water chemistry (pH, salinity, DO, turbidity, and temperature) (http://cwb.doh.hawaii.gov/CleanWaterBranch/WaterQualityData/default.aspx). However, the CWB sampling in the Ala Wai Canal has been suspended indefinitely due to budgetary constraints and *V. vulnificus* is not routinely monitored by the CWB anywhere in Hawai‘i. Previous studies investigating rain-driven effluent plumes from the canal suggest that the canal could be a source of pathogenic bacteria, including *V. vulnificus,* and pathogen indicator bacteria, specifically *Enterococcus* sp. (Connolly et al., 1999; Johnson et al., 2013) into coastal waters. *V. vulnificus* is found and regularly cultured from the canal and has been shown to vary over a seasonal cycle with little variation attributed to water temperature (Nigro, 2012). The variation in response to low salinity has been attributed to a strong correlation with groundwater flow (reduced nitrogen and silicate) rather than surface runoff (Nigro, 2012).

Field Surveys and Sample Collection

Biogeochemical survey data were collected over 9 sampling dates between October 2018

and October 2019 (21 October 2018; 29 November 2018; 20 January 2019; 18 February 2019; 22 March 2019; 20 April 2019; 4 June 2019; 31 August 2019; 29 September 2019). Depth profiles were collected from 18 sites along the Ala Wai canal and offshore (Figure 1.1). Continuous sensor profiles were conducted at each site on each date for salinity, temperature, turbidity, chlorophyll fluorescence, and dissolved oxygen. Discrete bottle samples were collected at 8 of these sites roughly 0.5 km apart along the transect. For discrete sampling, water was pumped into 1 L polycarbonate bottles at 3 depths per site: surface (25 cm below the air-water interface), middle (targeting the pycnocline), and bottom (25 cm above the sediment-water interface). Sampling was conducted sequentially along the sites and against the tidal flow over a period of ~3 h. I targeted sampling from the back of the canal at the lowest low tide for consistency and maximal gradient in salinity. Bottle samples were processed or preserved within 8 h of collection.

Hydrological and Climatological Data Sources

For each sampling date, Mānoa stream water height and discharge data were downloaded from the United States Geological Survey (USGS) National Water Information System (https://waterdata.usgs.gov/HI/nwis/current/?type=dailydischarge&group_key=basin_cd) for site 16240500 (21.328222˚N, -157.799611˚E). Tide data were downloaded from the National Oceanic and Atmospheric Administration (NOAA) Tides and Currents (https://tidesandcurrents.noaa.gov/datums.html?id=1612340) for site 1612340 (21.306667˚N, -157.866667˚E). Air temperature, wind speed, and precipitation data were downloaded from the NOAA National Centers for Environmental Information (https://www.ncdc.noaa.gov/cdo-web/search) Global Historical Climatology Network for site GHCND:US1HIHN0023 (21.300423˚N, -157.829327˚E).

Water Chemistry Data Collection

In Situ Sensor Data Collection

Temperature and conductivity were measured using an Aanderaa 4319A conductivity sensor (1.4 Hz). Dissolved oxygen was measured using an Aanderaa 4330F optode (~ 1 Hz). Turbidity (approximated from optical backscatter) and chlorophyll-a fluorescence were

measured using a Sea-Bird ECO FLNTU sensor (~ 6 Hz). Depth was measured using a custom-built water pressure probe (~ 1 Hz). Precise latitude and longitude were recorded using an onboard Simrad GPS.

Nutrient Measurements

All nutrient samples were analyzed at the University of Hawai‘i at Mānoa School of Ocean and Earth Science and Technology (SOEST) Laboratory for Analytical Biochemistry (http://www.soest.hawaii.edu/S-LAB/) using a Seal Analytical AA3 HR Nutrient Autoanalyzer. Dissolved nitrate plus nitrite, ammonium, phosphate, and silicate were analyzed according to Armstrong et al. (1967) and Grasshoff et al. (1983), Kérouel & Aminot (1997), Murphy & Riley, (1962), and Grasshoff et al. (1983), respectively, following filtration through a 0.22 μm pore size polyethersulfone filter capsule (Sterivex, Millipore) using a peristaltic pump. Total nitrogen and total phosphorus were measured from non-filtered samples following the modified Autoanalyzer procedure developed by the University of Hamburg.

Particulate and Dissolved Organics Measurements

Particulate organic carbon (POC) and particulate organic nitrogen (PON) samples were collected on combusted GF/F filters (Whatman) and analyzed using an Exeter Analytical model CE 440 elemental analyzer according to methods by Gordon (1969) and Sharp (1974). Filtrate was collected and acidified to pH 2 to measure dissolved organic carbon (DOC) and total dissolved nitrogen (TDN) using a Shimadzu High-Temperature TOC-L Combustion Analyzer. Samples for fluorescent dissolved organic matter (fDOM) were analyzed using a Horiba Aqualog scanning fluorometer according to Nelson et al. (2015). Relative fluorescence of known spectral peaks in excitation emission matrices was determined based on Coble (1996).

pH Measurements

Measurements of pH were made from whole water bottle samples in the lab using a Hach sensor probe calibrated for each sampling event.

Microbial Data Collection

Chlorophyll-a Measurements

Chlorophyll-a was measured from bottle samples using acetone extraction from material collected on 0.45 μm HAWP filters (Millipore) and fluorescence spectroscopy on a modified Turner 10AU fluorometer according to Smith et al. (1981) with a detection limit of 0.025 μg L^{-1} using the EPA Method 445.0.

Total Prokaryotic Abundance Measurements

Total prokaryotic abundance was determined using an Attune Acoustic Focusing Cytometer according to Nelson et al. (2015) from whole water samples fixed with paraformaldehyde (0.5% final concentration) and stained with 1X SYBR Green I.

DNA Extraction Protocol

Samples for DNA extraction were collected by passing water through 0.22 μm polyethersulfone filters (Sterivex, Millipore); the exact filtrate volume was recorded (250-500 mL). Filters were added to MP Biomedicals Lysing Matrix A (No. 116910100) tubes with MC 1 lysis buffer and homogenized using a MP Biomedicals FastPrep-96 bead beater. DNA extractions were completed using the Macherey-Nagel NucleoMag Plant Extraction Kit (No. 744400.4) with KingFisher accessory kit (No. 744951). Samples were eluted to a final volume of 110 μL.

Quantifying Vibrio vulnificus

There is a consistent log correlation between CHROMagar *Vibrio* blue colony forming units and *V. vulnificus* hemolysin A (*vvhA*) gene copy concentrations (Nigro & Steward, 2015). Therefore, I used a 16S rRNA 5' nuclease *vvhA* quantitative PCR assay (Campbell & Wright, 2003; Holland et al., 1991; forward primer: 5'-TGTTTATGGTGAGAACGGTGACA-3'; reverse primer: 5'-TTCTTTATCTAGGCCCCAAACTTG-3'; 5'-nuclease probe: 5'-/56-FAM/CCGTTAACC/ZEN/GAACCACCCGCAA/31ABkFQ/-3') to determine total *V. vulnificus* abundance. A 25 μL reaction mixture was prepared with final concentrations of 1X Kapa Probe Force Master Mix (Kapa Biosystems), 0.9 μM of each primer, 0.5 μM of the labeled probe, 0.56

mg/ml bovine serum albumin (Thermofisher), and 5 μL of DNA template (11.4 – 22.7 mL sample water). All qPCR reactions were performed in triplicate with the final replicate diluted 10-fold to check for inhibition of amplification as suggested by Bustin et al. (2009). The cycling protocol consisted of an initial denaturation step at 95 °C for 10 minutes, followed by 40 cycles of denaturation at 95 °C for 15 s and a combined annealing/extension at 60 °C for 30 minutes. I created an eight-point standard curve (10 – 50,000 copies per reaction well) of genomic DNA from *V. vulnificus* (strain YJ016; Chen et al., 2003) with known gene copy numbers per reaction run in triplicate along with the environmental samples. Assay efficiency was calculated from multiple standard curves using the formula $E = -1 + 10^{(-1/slope)}$ (Pfaffl, 2001).

Data Analysis

Data Processing

Data collected from sensors (salinity, temperature, dissolved oxygen, chlorophyll, and turbidity) were resampled to 1 Hz frequency with linear interpolation using Python 3.7.4 (Python Core Team, 2015) pandas package (McKinney, 2011) in order to coordinate the datasets based on timestamp. These data were then averaged over the time the bottle sample was collected to combine with discrete bottle measurements (nutrients, organics, pH, chlorophyll-a, total prokaryotes, *vvhA*). When necessary, data were transformed to a Gaussian distribution, typically via log10, to satisfy residual error distribution assumptions for linear regression statistical analysis. Replicate qPCR measurements of *vvhA* gene copy number were averaged and those below the assay limit of detection (10 copies per reaction) were set to the lowest detectable measurement of 0.1 copies mL^{-1} sample volume. *V. vulnificus* density values (*vvhA* gene copies mL^{-1}) were log_{10} transformed.

Statistical Analysis and Model Selection

I hypothesized that spatial and temporal variation in environmental parameters could explain significant variation in *V. vulnificus* density. In particular, I hypothesized that including additional measurements, such as nutrients and organics, in coordination with salinity and temperature could improve statistical models of *V. vulnificus* density in the Ala Wai Canal. To avoid collinearity between model predictors, I assessed pairwise correlation of all predictors to

generate a correlation matrix. A hierarchical cluster based on the correlation matrix was generated and one or two predictors were chosen from each major cluster (Figure 1.2) to be included in the full model for further analysis. To maximize the usefulness of the final model, I prioritized parameters that are widely measured, lower cost, and available on continuous monitoring platforms.

To test my hypothesis, I $\log_{10}$-transformed the response variable (*V. vulnificus* density) and fit a linear model with an error distribution assumption of normal. The model included main effects of predictors only with no interaction terms in order to maximize reproducibility in other systems. Model assumptions were assessed by inspection of residuals for normality and uniformity. Linear regression analyses were performed using R version 3.1.6 (R Core Team, 2019). The best combination of predictors was determined by fitting all possible predictor combinations using the dredge function in the MuMIn package (Bartoń, 2019) and comparing the Akaike Information Criterion value (Akaike, 1973) corrected for small samples sizes (AICc). The importance of predictors was evaluated using the importance function from the MuMIn package to get an importance measure of each predictor. The importance value is the sum of the model Akaike weights for all models that contain the particular parameter. Leave-one-out cross-validation was used to evaluate the prediction error (PE) of different models based on the root mean squared error (RMSE) of predictions versus observations, where PE is calculated as the $\log_{10}$-corrected RMSE.

Short-term Forecasting

Short-term forecasting, or nowcasting, of *V. vulnificus* density was developed using the PacIOOS nearshore sensor NS02 (http://www.pacioos.hawaii.edu/water/sensor-hawaiiyachtclub/) and the PacIOOS turbidity plume forecast (http://www.pacioos.hawaii.edu/water/model-plume-alawai/) based on the Regional Ocean Modeling System for the Waikīkī area (Waikīkī ROMS). The PacIOOS NS02 is moored at 1 m depth at (21.286407˚N, -157.84276˚E) and records continuous measurements of temperature and conductivity (Sea-Bird Electronics, SBE16*plus* V2 SEACAT), and fluorescence (470/695 nm) from which chlorophyll-a is estimated, and optical backscatter (700 nm) as an approximation of turbidity (WET Labs, ECO FLNTUS) at 0.0042 Hz frequency (McManus, 2008). An additional

sensor for continuous measurements of fDOM (WET Labs, WETStar DOM Fluorometer, 370 nm excitation/460 nm emission, 0.0014 Hz; Belzile et al., 2006) was deployed at this location from September 2018 – May 2019. These measurements were validated based on depth profile measurements in this study at site 2. *V. vulnificus* density was predicted using NS02 salinity, National Weather Service five-day average rainfall and daily maximum air temperature and compared to measured *V. vulnificus* density. Air temperature and water temperature are highly correlated, so air temperature was used since it is easier to measure remotely. A second model of *V. vulnificus* density which included fDOM measurements was compared to the previous model to assess the effect of adding DOM as a model parameter. Goodness of fit and model prediction error were evaluated by RMSE.

The PacIOOS turbidity plume forecast based on the Waikīkī ROMS predicts three-dimensional circulation as well as salinity, temperature, and turbidity based on the PacIOOS NS02 measurements for the canal and adjacent coastal region. The model is spatially resolved within the canal and nearshore environment to 40 m with 14 depth layers (0.25, 1, 2, 5, 10, 20, 30, 50, 75, 100, 125, 150, 200, 250 m) at 1 h time intervals. *V. vulnificus* density was predicted for the surface 0.25 m depth using the forecasted salinity and turbidity, and NWS five-day average rainfall, and daily maximum air temperature.

Long-term Forecasting

End-of-century projections of air temperature and precipitation were used to estimate overall change in *V. vulnificus* density due to climate change. The dynamical downscaling projections that were used (Zhang et al., 2012, 2016a, 2016b) are based on the IPCC AR5 CMIP5 global model for representative concentration pathways (RCP) 4.5 and 8.5 (IPCC, 2014). The forecasting assumes a linear response of *V. vulnificus* with increasing temperature and no significant changes to other aspects of environmental variation.

1.4 RESULTS

Spatial and Temporal Variation of V. vulnificus

V. vulnificus density (*vvhA* gene copies mL^{-1}) ranged from 0.1 – 266 with a geometric mean of 4.0 for the warm, rainy season (October – March) and ranged from 0.1 – 529 with a geometric mean of 17.6 for the hot, dry season (April – September). There were significant differences between month ($F = 18.24$, $p < 0.001$), site ($F = 8.88$, $p < 0.001$), and depth ($F = 26.80$, $p < 0.001$) in *V. vulnificus* density (Figure 1.3). *V. vulnificus* density was significantly elevated in the surface water, within the canal (sites 1 – 6), and during the summer months.

Correlation with Biogeochemical Predictors

V. vulnificus density was most strongly correlated with dissolved inorganic nutrient concentrations and metrics of fluorescent DOM characteristics (Figure 1.2; $r > 0.6$). The strongest additional univariate correlations ($r > 0.4$) were rainfall, total prokaryotes, turbidity (Figure 1.4), and bulk measurements of dissolved and particulate organic carbon and nitrogen. *V. vulnificus* concentrations were strongly negatively correlated ($r < - 0.4$) with pH and salinity. I found no significant correlation between *V. vulnificus* ($p < 0.05$) and stream discharge and *V. vulnificus* and chlorophyll-a measured *in situ*.

Predictive Model Selection

To construct predictive models, highly correlating biogeochemical parameters were removed to mitigate overfitting, unstable coefficient estimates, and high prediction error. I prioritized parameters that are widely measured, lower cost and available on continuous monitoring platforms. Out of 36 biogeochemical measurements, 12 were chosen for model selection analysis, with 1-2 parameters each representing one of 9 clusters of covarying parameters (Figure 1.2). Five-day average rainfall, daily maximum air temperature, salinity, turbidity, dissolved oxygen, particulate organic carbon, silicate, phosphate, visible humic-like fDOM, the fDOM humification index (HIX), and total prokaryote density had reasonably low pairwise collinearity and were used as terms to construct a linear model of *V. vulnificus* density in $\log_{10}$(*vvhA* gene copies mL^{-1}) (Table 1.1). Model residuals were well-behaved (uniformly

distributed relative to predicted values) and normally distributed, following model assumptions. For the full model with all terms, the residual standard error was 0.54 on 179 degrees of freedom with an R^2 value of 0.70.

Comparing models representing all combinations of predictors, 24 models were within $\Delta AICc < 4$ of the best-specified model and rainfall, air temperature, salinity, silicate, visible humic-like fDOM, and HIX were included in all 24 of those low AICc models. The best-specified model based on AICc included rainfall, air temperature, salinity, dissolved oxygen, silicate, visible humic-like fDOM, and HIX had an R^2 of 0.70 (Model 6 in Table 1.2). The second lowest AICc model ($\Delta AICc = 1.03$, $R^2 = 0.69$) does not include dissolved oxygen. The importance value for each predictor, calculated using the MuMIn package, is reported in Table 1.1.

Operational Model Comparison and Cross Validation

Based on the important predictors from the best-specified model (see *Predictive Model Selection*) and model applications (see *Model Forecasting Applications*), six linear regression models were compared to assess predictive power of *V. vulnificus* density (Table 1.2, Figure 1.5). The models were compared using AICc and RMSE as well as the average RMSE from LOOCV to assess model fit and prediction error. ΔAICc is relative to model 6, the best-specified model. As RMSE is the average error between the predicted and observed value, the "prediction error" is the log-corrected RMSE. Model 1 included rainfall and air temperature only as predictors of *V. vulnificus* density and performed the worst ($R^2 = 0.325$, $\Delta AICc = 140$, RMSE = 0.79, LOOCV RMSE = 0.80, Prediction Error = 6.3). Model 2 included water chemistry parameters: salinity and water temperature. Model 2 performed better than model 1 and explains more variation in *V. vulnificus* density ($R^2 = 0.46$, $\Delta AICc = 96$, RMSE = 0.70, LOOCV RMSE = 0.71, Prediction Error = 5.1). Model 3 combined climate and water chemistry parameters: rainfall, air temperature, and salinity. Water temperature was removed to avoid collinearity with air temperature and air temperature explained slightly more variation in *V. vulnificus* density as well as being easier to measure remotely. Model 3 performed better than model 2 and explains more variation in *V. vulnificus* density ($R^2 = 0.53$, $\Delta AICc = 71$, RMSE = 0.67, LOOCV RMSE = 0.67, Prediction Error = 4.7). Model 4 builds from model 3 to include turbidity which is modeled

in the Waikīkī ROMS forecast. Again, model 4 performed better than model 3 and explains more variation in *V. vulnificus* density (R^2 = 0.58, ΔAICc = 55, RMSE = 0.63, LOOCV RMSE = 0.64, Prediction Error = 4.4). Model 5 replaces turbidity with visible humic-like fDOM which is measured at the NS02 time series. Model 5 performed better than model 4 and explains more variation in *V. vulnificus* density (R^2 = 0.62, ΔAICc = 34, RMSE = 0.59, LOOCV RMSE = 0.61, Prediction Error = 4.1). Model 6, is the best-specified model from model selection analysis and performed as such (R^2 = 0.69, ΔAICc = 0, RMSE = 0.53, LOOCV RMSE = 0.55, Prediction Error = 3.6).

Model Forecasting Applications

Short-term Forecasting

The PacIOOS time series data from NS02 were validated against measured observations in this survey from site 2 (Figure 1.6). Overall, the NS02 data were roughly equivalent to the survey data with high R^2 values and a linear fit with intercepts near zero and slopes near one. Salinity and turbidity are exceptions with salinity R^2 of 0.41, attributable to fine-scale variation in sampling location in a stratified estuarine habitat, and turbidity having an intercept of 2.1 potentially caused by an instrument offset. Using the NS02 data, *V. vulnificus* density was hindcast for the sampling period (Figure 1.7) and validated against measured observations (Figure 1.8). Two model frameworks were compared to assess the improvement of adding fDOM measurements (model 3 vs. model 5, see *Operational Model Comparison*). Model 3 ("– fDOM") uses salinity, five-day average rainfall, and daily maximum air temperature to predict *V. vulnificus* density (R^2 = 0.53) with RMSE of 0.33 and R^2 of 0.53 compared to measured values. Model 5 ("+ fDOM") uses salinity, five-day average rainfall, daily maximum air temperature, and visible humic-like fDOM to predict *V. vulnificus* density (R^2 = 0.62) with RMSE of 0.12 and R^2 of 0.98 compared to measured values. The addition of fDOM measurements in Model 5 improves predictions of *V. vulnificus* density (Figure 1.8).

A three-day spatial forecast of *V. vulnificus* density was constructed using the PacIOOS turbidity plume forecast and Waikīkī ROMS model framework which includes 4 m resolution projections of salinity, temperature, and turbidity in addition to water velocity at 1 h intervals. Model 4 (see *Operational Model Comparison*) was used to predict *V. vulnificus* density based on

the forecast output. For an example rain event in February 2019, this model demonstrated *V. vulnificus* plume dynamics exiting the Ala Wai Canal (Figure 1.9).

Long-term Forecasting

Long-term climate predictions were based on Model 1, rainfall and air temperature, using projections of monthly average rainfall and air temperature. Model 1 was first validated against survey measurements of *V. vulnificus* density (Figure 1.10). The climate model does not accurately predict the spatial variation in *V. vulnificus* density ($R^2 = 0.42$, RMSE = 0.65, PE = 4.47), but does well to predict the overall average *V. vulnificus* density within the canal ($R^2 = 0.90$, RMSE = 0.04, PE = 1.1). Model coefficients were used to predict the long-term effects of changing rainfall and air temperature on overall average *V. vulnificus* density for the canal. Three climate projections were considered based on dynamical downscaling (250 m resolution) of recorded data (1990-2009) and the AR5 RCP 4.5 and RCP 8.5 modeled scenarios (2080-2099). RCP 4.5 is a 580-720 ppm CO2-eq by 2100 and 1.7-3.2 °C increase relative to 1850-1900 and RCP 8.5 is a >1000 ppm CO2-eq by 2100 and 3.2-5.4 °C increase relative to 1850-1900. There was no significant difference ($p = 0.45$) in annual average rainfall between the three projections (1990-2009, RCP 4.5, and RCP 8.5) (Figure 1.11). There was a significant difference ($p < 0.0001$) in annual average air temperature between the three projections. Mean comparisons using Tukey-Kramer HSD show that RCP 8.5 (mean = 27.6 °C) is significantly higher ($p < 0.0001$) than RCP 4.5 (mean = 26.0 °C) and RCP 4.5 is significantly higher ($p < 0.0001$) than 1990-2009 (mean = 24.2 °C). There is also a significant difference ($p < 0.0001$) in predicted annual average *V. vulnificus* density between the three projections (Figures 1.11 and 1.12). Mean comparisons using Tukey-Kramer HSD show that RCP 8.5 (mean = 61.0 vvhA gene copies mL^{-1}) is significantly higher ($p < 0.0001$) than RCP 4.5 (mean = 36.5 vvhA gene copies mL^{-1}) and RCP 4.5 is significantly higher ($p < 0.0001$) than 1990-2009 (mean = 19.3 vvhA gene copies mL^{-1}). The RCP 4.5 and 8.5 values in *V. vulnificus* density correspond to a 21.5 % and 38.9 % increase respectively relative to 1990-2009 (Figure 1.12).

1.5 DISCUSSION

General Patterns in **Vibrio vulnificus** *Seasonality*

Hawai‘i has consistently higher *Vibrio* infection rates per capita than any other state in the U.S. This study evaluates statistical models of *V. vulnificus* concentrations in the Ala Wai Canal, a tropical estuarine environment in a densely populated area of Honolulu, Hawai‘i. The results demonstrate how accounting for spatiotemporal dynamics of dissolved nutrient resources improves the predictive capabilities of these statistical models and model applications. Despite the high degree of both temporal and spatial variation, climate and biogeochemistry can explain up to 70 % of the variation in *V. vulnificus* density using the best-specified model (Model 6 in Table 1.2). There is a significant increase in *V. vulnificus* density in the summer months which corresponds with higher water temperatures and an enhanced chlorophyll density likely generating the observed increase in dissolved oxygen and organic matter (Figure 1.4). These results contrast previous findings in the canal from a decade prior (Nigro, 2012) which show overall higher abundances during the rainy season and may reflect changes to the environment such as increasing water temperature in the summer months over 10 years or differences in the rain events captured between the studies. Rain events, which transport nutrients and dissolved organics as well as low salinity water into the canal through the streams and runoff are also positively correlated with *V. vulnificus* density in this study (see the February 2019 rain event in Figures 1.3 and 1.9). These findings are consistent with a previous survey that show elevated concentrations of *V. vulnificus* in the harbor region after a large rain event (Nigro, 2012). These results suggest that conditions for *V. vulnificus* growth are improved in this outflow region during rain events in addition to water movement transporting *V. vulnificus* out of the canal. Since the harbor and outflow regions are sites of high and concentrated recreational activity, summer rain storms may be particularly concerning for human exposure to *V. vulnificus*. Interestingly, Fiedler et al. (2014) also reported a significant increase in *V. vulnificus* density near the PacIOOS NS02 following the Japan tsunami. The correlation and importance of SiO_2 (De Carlo et al., 2007) and HIX (Nelson et al., 2015) in the modeling exercises suggests a positive response of *V. vulnificus* to groundwater flow which is in keeping with the findings of Nigro (2012).

The pattern and order-of-magnitude seasonal variation in *V. vulnificus* density recorded in this study is comparable to previous studies in other areas (Jacobs et al., 2014; Pfeffer et al., 2003; Tamplin et al., 1982), but significantly lower than previous reports in the Ala Wai Canal where canal-wide average concentrations ranged from 23.1 *vvhA* gene copies mL^{-1} to 3640 *vvhA* gene copies mL^{-1} (Nigro, 2012). This variation is still notable since the water temperature remains well above the 18 °C minimum for optimal growth (ranging between 22 – 31 °C). For this environment, salinity and temperature alone explain only 20 – 30 % of the variation in *V. vulnificus* density.

Improvements with Dissolved Nutrients and Organics

The quality of nutrient resources available may be an important and overlooked determinant in predicting the population dynamics of *V. vulnificus*. My results indicate that the addition of fluorescent dissolved organic matter (fDOM) measurements to resolve humic components (often targeting a range of wavelengths referred to as "cDOM" or visible humic-like components; Nelson & Siegel, 2013) could resolve 10 % more variation in *V. vulnificus* density than salinity and climate parameters alone (Model 3 vs. 5 in Table 1.2). In application, the addition of a real time deployed fDOM sensor at NS02 reduced prediction error by 36 % (Figure 1.8). Although dissolved inorganic nutrients, particularly silicate, are also important in the models and strongly correlated with *V. vulnificus* concentrations, nutrient analysis currently requires water sample collection and laboratory analysis. Fluorescent DOM can be measured with a deployed real time sensor and fDOM parameters were almost equally correlated with *V. vulnificus* as nutrients were with *V. vulnificus* (Figure 1.2). However, advances are being made in real-time sensors for inorganic nutrients such as nitrate (Sea-Bird Scientific, SUNA V2 Nitrate Sensor based on Johnson & Coletti, 2002) and orthophosphate (Sea-Bird Scientific, HydroCycle-Phosphate Analyzer). These real-time sensors may become valuable tools for future coastal pathogen monitoring programs.

There are only a few studies on natural populations of *V. vulnificus* in tropical estuaries. In the case of a tropical environment where temperature is always facilitating rather than limiting growth, other factors, such as macronutrient resource abundance and quality, may be more important controls on the population density of *V. vulnificus*. Vibrios are copiotrophic

bacterioplankton with broad capacity to degrade organic compounds and extract macronutrients from DOM (Baker-Austin et al., 2018). As such, the character and quantity of DOM is a reasonable parameter modulating growth dynamics of this pathogen and other naturally-occurring estuarine organisms. Considering nutrient and DOM resources in predictive modeling seems to be a promising route forward. Measurements of fluorescent dissolved organic matter, which can be recorded easily with deployed sensors (Belzile et al., 2006; Carstea et al., 2020; Ruhala & Zarnetske, 2017), may be the key to generating robust predictive models of *V. vulnificus* population dynamics. There are even promising efforts at forecast modeling DOM in estuarine environments (Bowers & Brett, 2008) which could be integrated into coastal pathogen modeling.

Conclusions and Climate Change Implications

This study parameterizes *V. vulnificus* absolute abundance with comprehensive physical, optical, and chemical water properties in high spatial and temporal resolution to develop a real-time spatially-explicit model of *V. vulnificus* pathogen risk. It is critical that we improve our predictive capabilities of the *V. vulnificus* human pathogen in the face of increased water temperature, storm surge, sea level, hurricanes, and flooding due to climate change which may be favorable to *V. vulnificus*. The habitat range of *V. vulnificus* may expand due the sea level rise and coastal flooding given its preference for mixed salinity water. In addition, *V. vulnificus* population growth will likely increase due to increasing water temperature. There is evidence for significantly increased season length and spatial habitat from work in the Chesapeake Bay (Muhling et al., 2017). Based on local dynamical downscaling of the CMIP5 global model projections for rainfall and air temperature (Zhang et al., 2012, 2016a, 2016b), my models suggest a 21.5 – 38.9 % increase in average *V. vulnificus* density by 2100 if atmospheric CO_2 concentrations reach between RCP 4.5 and 8.5. If climate change proves more favorable for *V. vulnificus* and expands areas of coastal flooding, we will likely see increased exposure of the general public to *V. vulnificus* and increased infections. Therefore, improving predictive models of microbial pathogen populations is critical to public safety and incorporating real time measurements of nutrient resources may be a crucial step forward.

1.6 TABLES

Table 1.1 Model Selection: Full-model likelihood ratio test based on linear least squares regression analysis of *V. vulnificus* density in $\log_{10}$(*vvhA* gene copies mL^{-1}) and AIC-weighted importance of predictors based on model comparison of all possible predictor combinations.

Model Term	Coefficient Estimate	Standard Error	t-value	p-value		AIC-weighted Importance
(Intercept)	5.78E-02	1.17E+00	0.05	9.61E-01		NA
1. Five-day Average Rainfall	3.11E-01	5.15E-02	6.03	9.00E-09	***	1.00
2. DOM Humification Index	-2.25E-01	5.12E-02	-4.39	1.93E-05	***	1.00
3. Air Temperature	8.02E-02	2.05E-02	3.91	1.31E-04	***	1.00
4. Visible Humic-like DOM	1.13E+00	3.90E-01	2.89	4.31E-03	**	1.00
5. Silicate	5.11E-01	2.00E-01	2.56	1.13E-02	*	1.00
6. Salinity	-1.48E-05	6.34E-06	-2.34	2.04E-02	*	1.00
7. Dissolved Oxygen	-2.52E-02	1.66E-02	-1.51	1.31E-01		0.61
8. Particulate Organic Carbon	-1.13E-01	1.67E-01	-0.68	5.00E-01		0.33
9. Phosphate	-1.87E-01	2.06E-01	-0.91	3.70E-01		0.27
10. Total Prokaryotes	-7.61E-02	1.92E-01	-0.40	6.91E-01		0.19
11. Nitrate + Nitrite	3.52E-02	1.51E-01	0.23	8.16E-01		0.14
12. Turbidity	9.98E-04	1.36E-01	0.01	9.94E-01		0.14

Significance codes: 0 '***' 0.001 '**' 0.01 '*' 0.05 '.'

Table 1.2 Operational Model Comparison: Linear least squares regression analysis of *V. vulnificus* density in $\log_{10}$(vvhA gene copies mL^{-1}) comparing six models using AIC model selection analysis and root-mean-square-error (RMSE) for both the full dataset and leave-one-out-cross-validation (LOOCV).

Model 1 "Climate-only"	R^2 = 0.325	AICc = 464	RMSE = 0.79	LOOCV RMSE = 0.80	PE = 6.31
	Estimate	*SE*	*t value*	*p-value*	
(Intercept)	-4.00E+00	7.42E-01	-5.35	2.50E-07	***
Five-day Average Rainfall	4.41E-01	5.85E-02	7.55	1.80E-12	***
Air Temperature	1.42E-01	2.45E-02	5.85	2.10E-08	***
Model 2 "Water Chemistry"	R^2 = 0.462	AICc = 420	RMSE = 0.70	LOOCV RMSE = 0.71	PE = 5.13
	Estimate	*SE*	*t value*	*p-value*	
(Intercept)	-2.88E+00	7.26E-01	-3.97	1.00E-04	***
Salinity	-4.68E-05	4.54E-06	-10.3	<2.00E-16	***
Water Temperature	1.88E-01	2.63E-02	7.15	1.80E-11	***
Dissolved Oxygen	-4.04E-02	1.93E-02	-2.10	3.74E-02	*
Model 3 "Climate + Chemistry"	R^2 = 0.534	AICc = 395	RMSE = 0.66	LOOCV RMSE = 0.67	PE = 4.68
	Estimate	*SE*	*t value*	*p-value*	
(Intercept)	-2.65E+00	6.34E-01	-4.17	4.60E-05	***
Five-day Average Rainfall	3.17E-01	5.05E-02	6.28	2.30E-09	***
Air Temperature	1.41E-01	2.02E-02	6.96	5.60E-11	***
Salinity	-4.05E-05	4.40E-06	-9.22	<2.00E-16	***
Model 4 "ROMS"	R^2 = 0.576	AICc = 379	RMSE = 0.63	LOOCV RMSE = 0.64	PE = 4.37
	Estimate	*SE*	*t value*	*p-value*	
(Intercept)	-2.11E+00	6.19E-01	-3.41	7.90E-04	***
Five-day Average Rainfall	3.14E-01	4.83E-02	6.49	7.50E-10	***
Air Temperature	1.15E-01	2.03E-02	5.66	5.60E-08	***
Salinity	-3.69E-05	4.29E-06	-8.61	2.90E-15	***
Turbidity	4.76E-01	1.11E-01	4.30	2.70E-05	***

Table 1.2 (Continued).

Model 5 "NS02"	R^2 = 0.620	AICc = 358	RMSE = 0.59	LOOCV RMSE = 0.61	PE = 4.07
	Estimate	*SE*	*t value*	*p-value*	
(Intercept)	-1.40E+00	6.05E-01	-2.32	2.14E-02	*
Five-day Average Rainfall	3.17E-01	4.58E-02	6.93	6.50E-11	***
Air Temperature	1.13E-01	1.88E-02	6.01	9.20E-09	***
Salinity	-1.81E-05	5.27E-06	-3.44	7.30E-04	***
Visible Humic-like	8.94E-01	1.37E-01	6.51	6.60E-10	***

Model 6 "Best"	R^2 = 0.692	AICc = 324	RMSE = 0.53	LOOCV RMSE = 0.55	PE = 3.55
	Estimate	*SE*	*t value*	*p-value*	
(Intercept)	-1.62E-01	8.28E-01	-0.20	8.50E-01	
Five-day Average Rainfall	2.97E-01	4.58E-02	6.49	7.60E-10	***
Air Temperature	7.23E-02	1.83E-02	3.94	1.10E-04	***
Salinity	-1.63E-05	6.15E-06	-2.66	8.57E-03	**
Silicate	4.76E-01	1.40E-01	3.40	8.30E-04	***
Visible Humic-like DOM	9.04E-01	2.10E-01	4.31	2.60E-05	***
DOM Humification Index	-2.08E-01	4.25E-02	-4.88	2.20E-06	***
Dissolved Oxygen	-2.79E-02	1.63E-02	-1.71	8.81E-02	.

AICc is the Akaike Information Criterion value corrected for small sample sizes. RMSE is the average error between the predicted and observed value. LOOCV is the leave-one-out-cross-validation technique to test for prediction error. PE, or prediction error, is the log-corrected RMSE. SE is the standard error value from the likelihood ratio test. Significance codes: 0 '***' 0.001 '**' 0.01 '*' 0.05 '.'

1.7 FIGURES

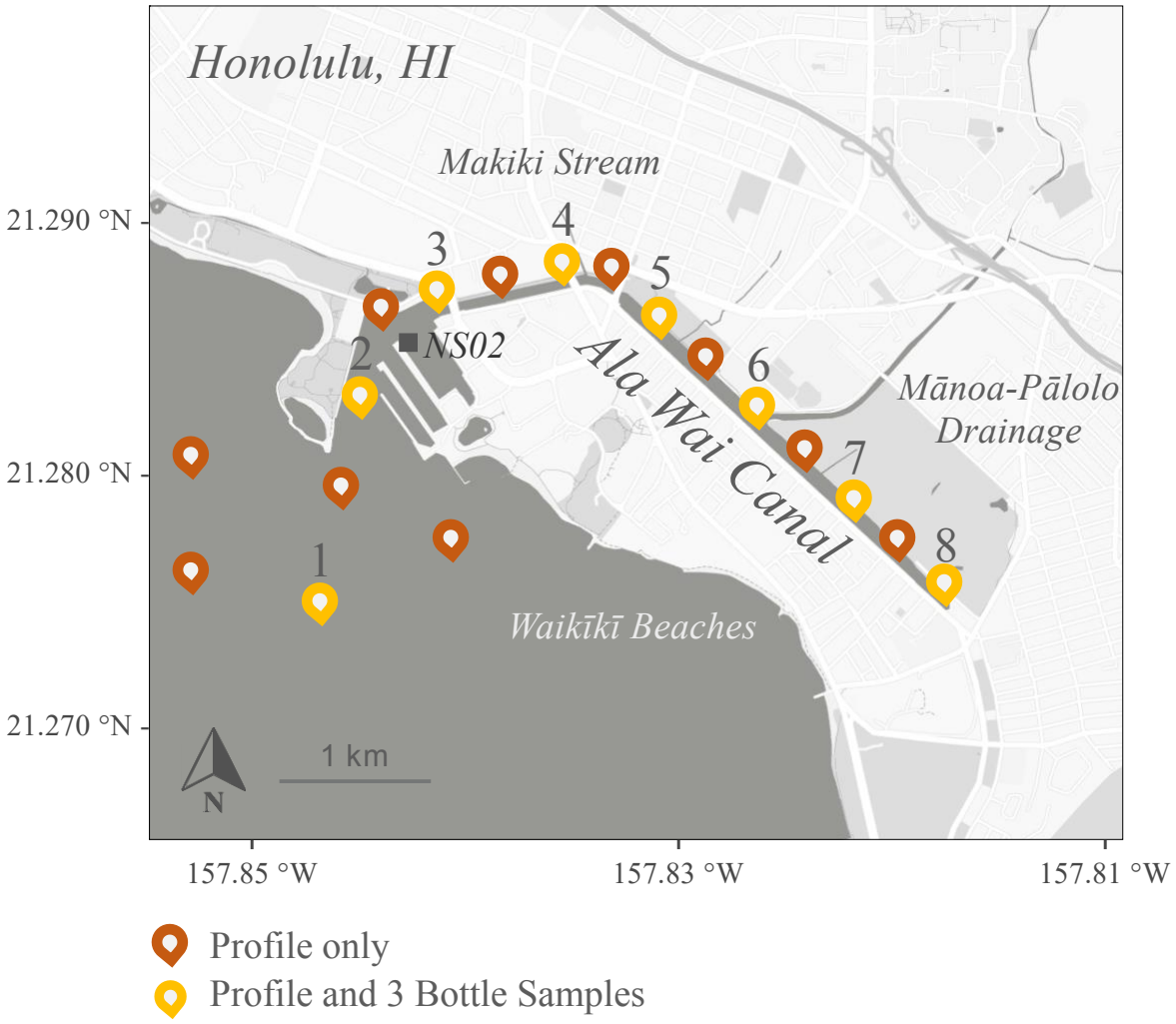

Figure 1.1 Map of the Ala Wai Canal in Honolulu, Hawai‘i depicting monthly survey sampling locations from October 2018 - September 2019. Full depth profiles for salinity, temperature, dissolved oxygen, turbidity, and chlorophyll were collected from all sites (n = 18) marked with a pin. Yellow numbered sites (1-8) are locations where discrete bottle samples were collected at three depths (surface, pycnocline, and bottom water) for additional nutrient, organic matter, and microbial measurements. The PacIOOS nearshore sensor NS02 at the Ala Wai Harbor is marked with a grey box.

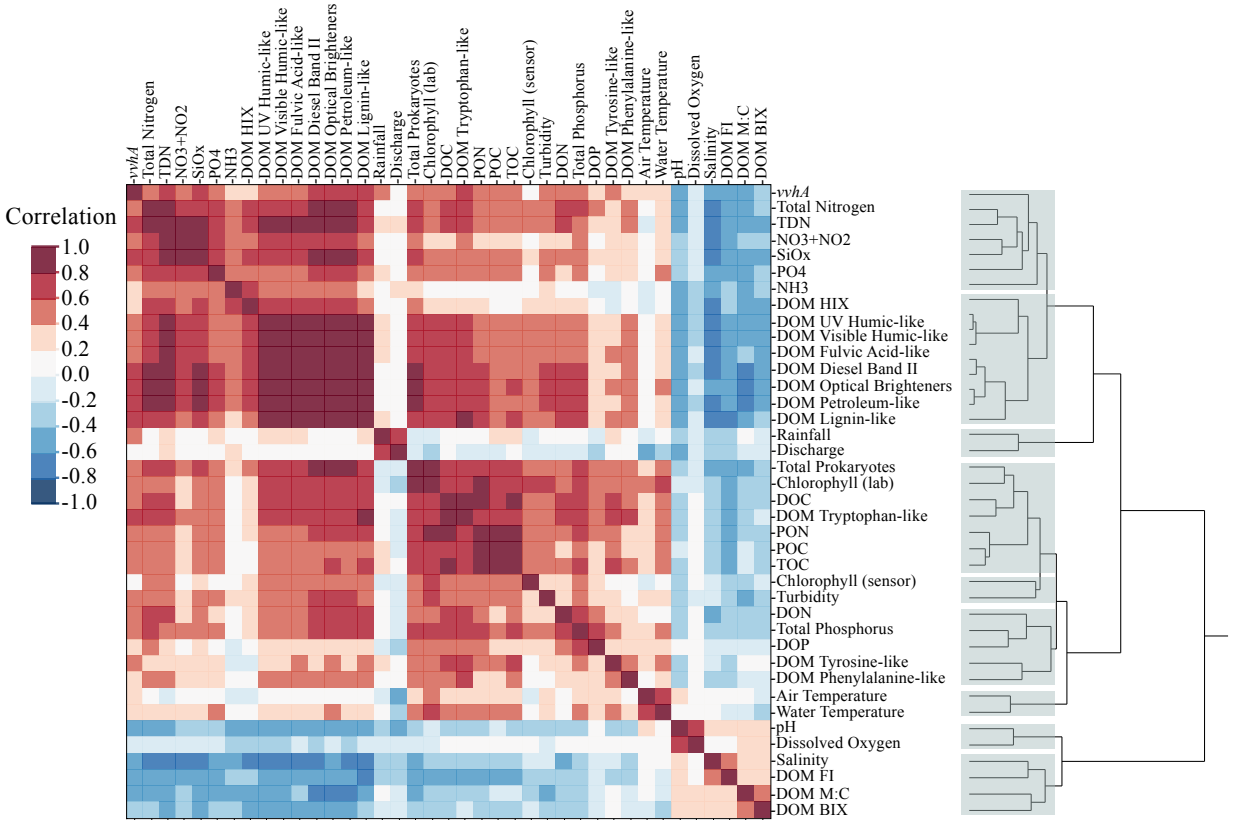

Figure 1.2 Heat map of the correlation matrix showing pairwise correlation of all variables. The dendrogram (right) depicts the hierarchical cluster structure based on the correlation matrix values. Light grey rectangles overlaying the dendrogram mark the nine major clusters of highly collinear variables.

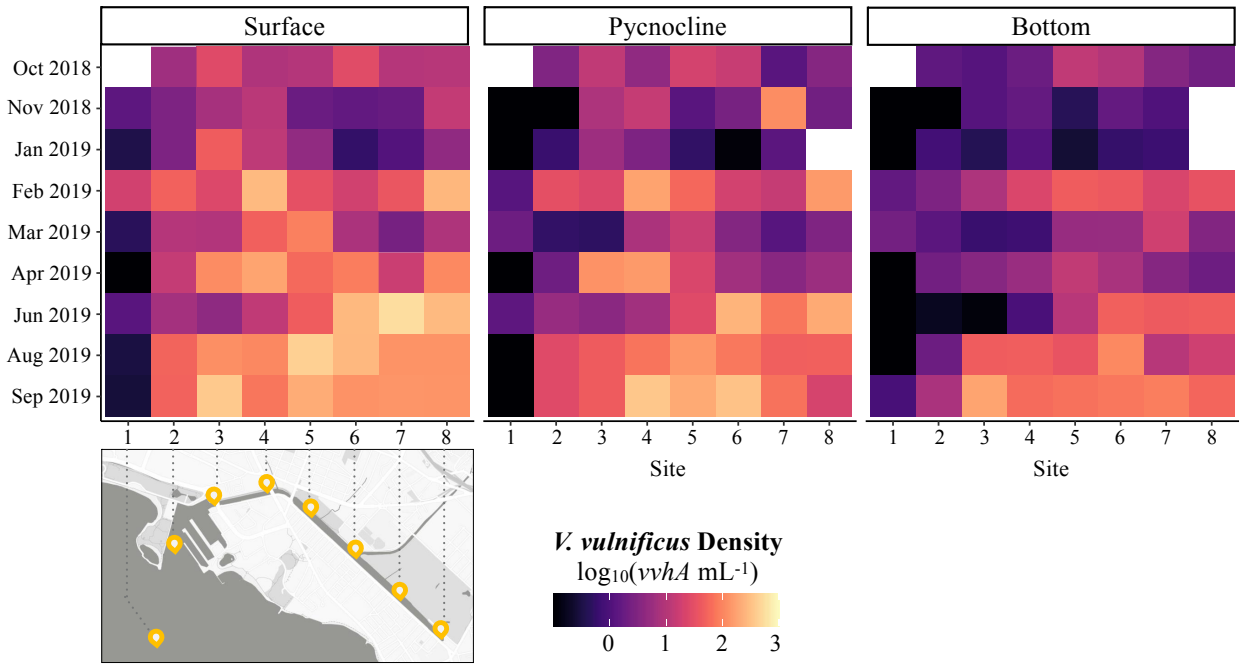

Figure 1.3 Spatial and temporal variation of *V. vulnificus* density in the Ala Wai Canal in Honolulu, Hawai‘i from October 2018 - September 2019 divided by site (horizontal axis) and sample depth (panels). *V. vulnificus* density varies significantly between months, sites, and depths ($p < 0.001$). *V. vulnificus* density significantly increases from offshore (site 1) to the back end of the canal (site 8) and in the surface waters (0.25 m from the surface) relative to the pycnocline or bottom waters (0.25 m from the bottom). Seasonally, canal-averaged *V. vulnificus* density rises through the year beginning in October 2018 and peaks in September 2019 with anomalously elevated levels during the February 2019 rain event.

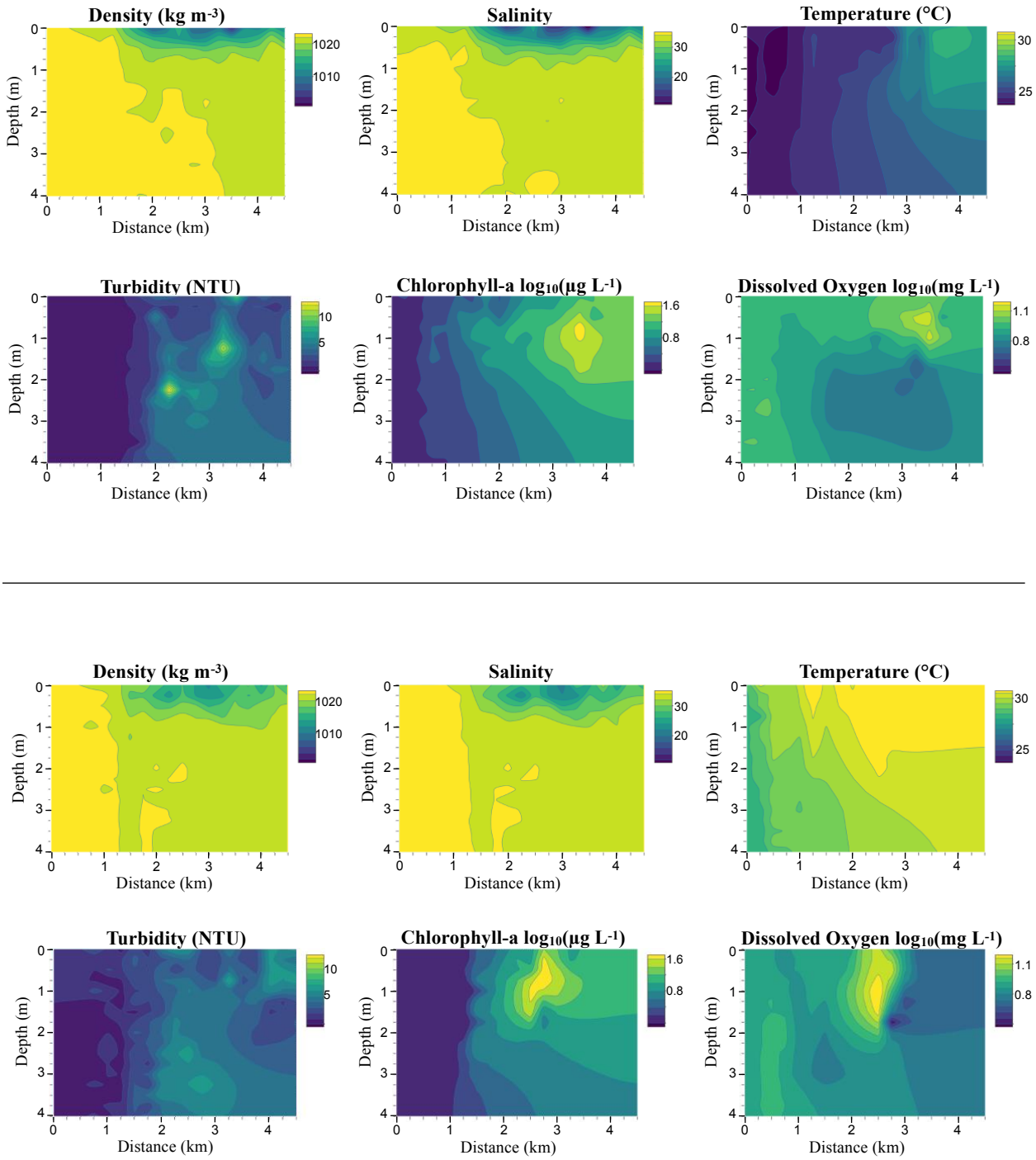

Figure 1.4 Continuous depth profiles of biogeochemistry in the Ala Wai Canal from October 2018 – September 2019. Data are separated by the rainy season (October through March; top set of panels) and the dry season (April through September; bottom set of panels).

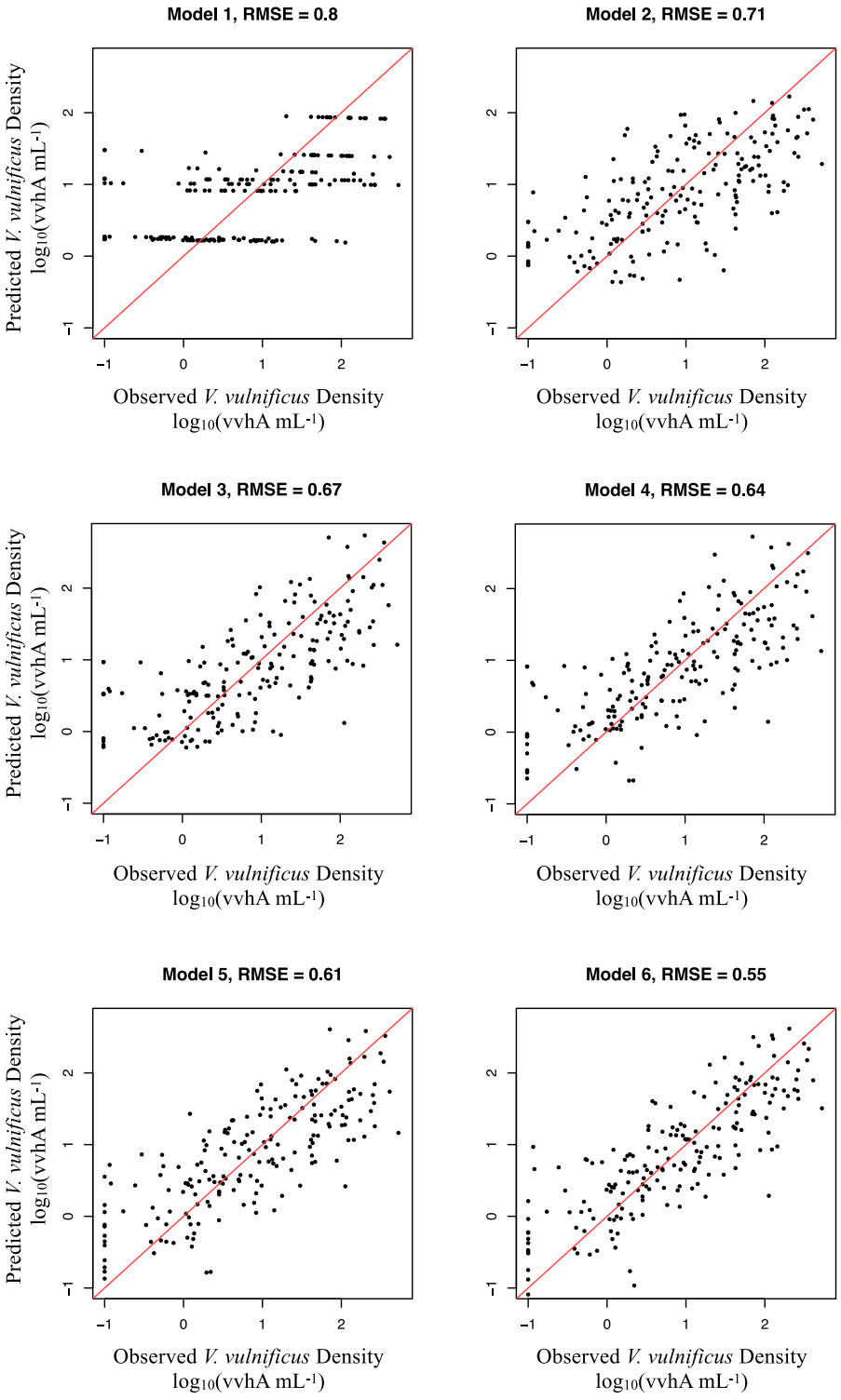

Figure 1.5 Operational Model Comparison. Model predictions, based on leave-one-out-cross-validation (LOOCV), are compared to observations of *V. vulnificus* density in $\log_{10}$(*vvhA* gene copies mL^{-1}) (see Table 1.2). The 1:1 line is in red. RMSE is the root mean squared error.

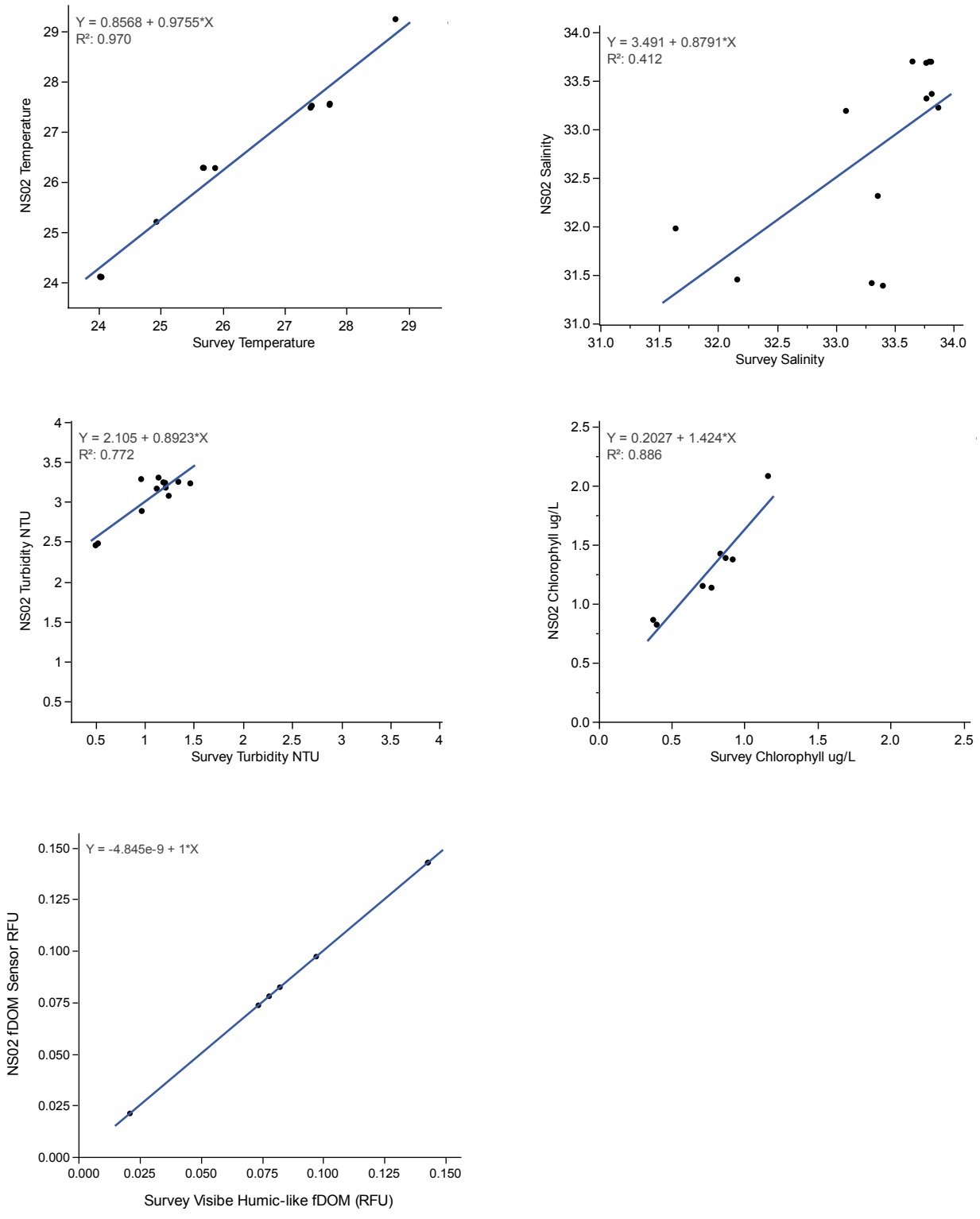

Figure 1.6 Validation of NS02 measurements with survey data from site 2 surface values. Linear fit equations are shown.

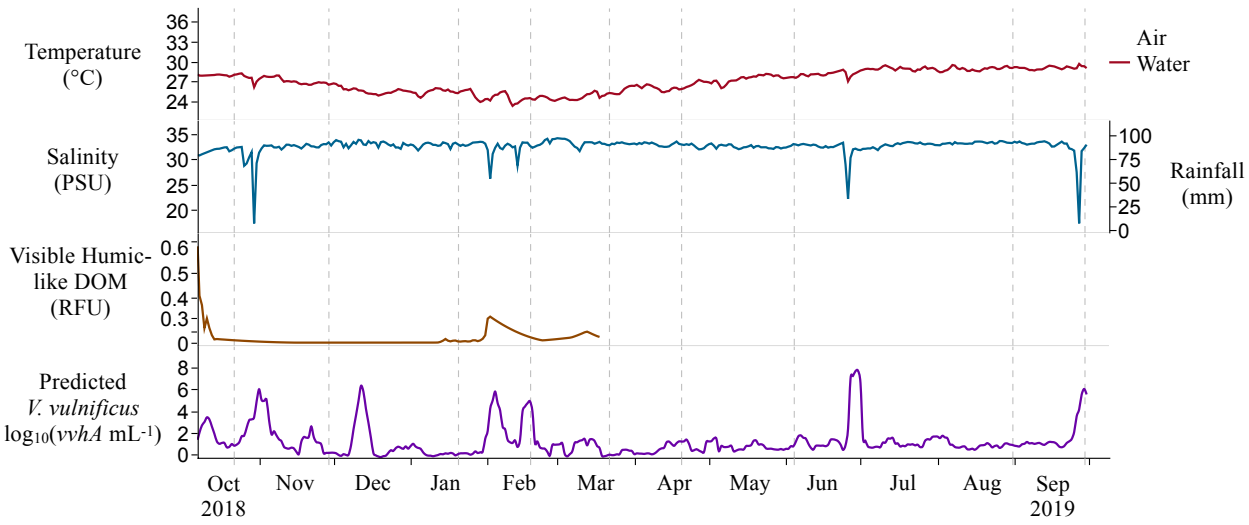

Figure 1.7 Time series of data from PacIOOS NS02, USGS, and NOAA National Weather Service. *V. vulnificus* density is hindcast using a linear model of five-day average rainfall, air temperature, salinity, and visible humic-like DOM (when data were available). Grey vertical dashed lines mark dates when field surveys were conducted.

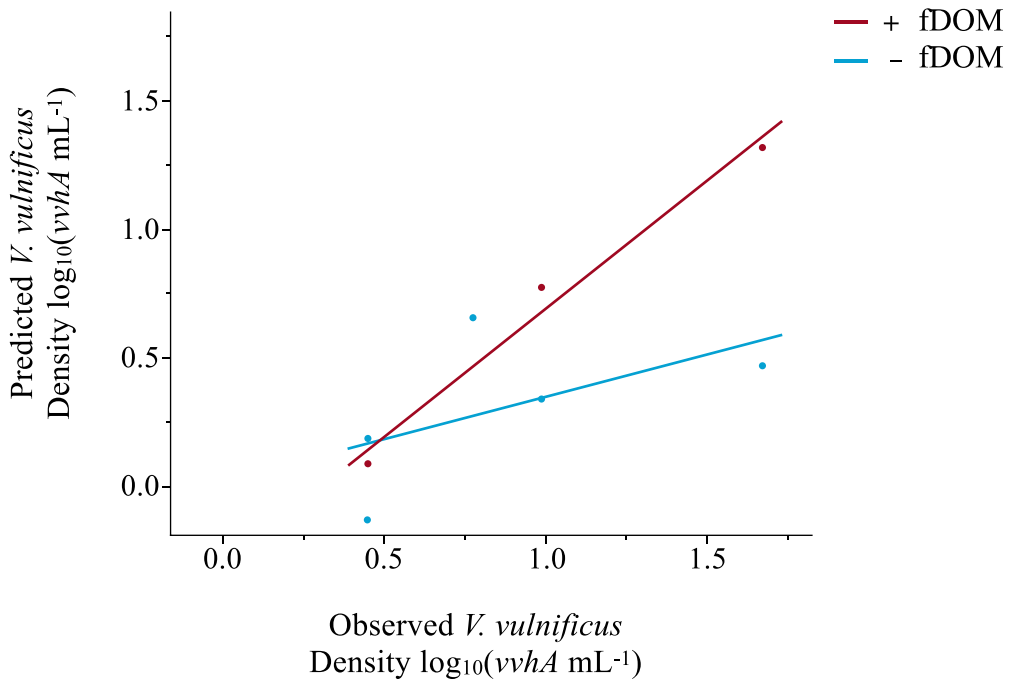

Figure 1.8 Predicted *V. vulnificus* density based on two models (see Model 3 and Model 5, Table 1.2) of NS02 data compared to measured *V. vulnificus* density from the survey site 2 surface values. Model 3 (– fDOM) uses salinity, five-day average rainfall, and daily maximum air temperature to predict *V. vulnificus* density ($R^2 = 0.53$) with RMSE of 0.33 and R^2 of 0.53 compared to measured values. Model 5 (+ fDOM) uses salinity, five-day average rainfall, daily maximum air temperature, and visible humic-like fDOM to predict *V. vulnificus* density ($R^2 = 0.62$) with RMSE of 0.12 and R^2 of 0.98 compared to measured values.

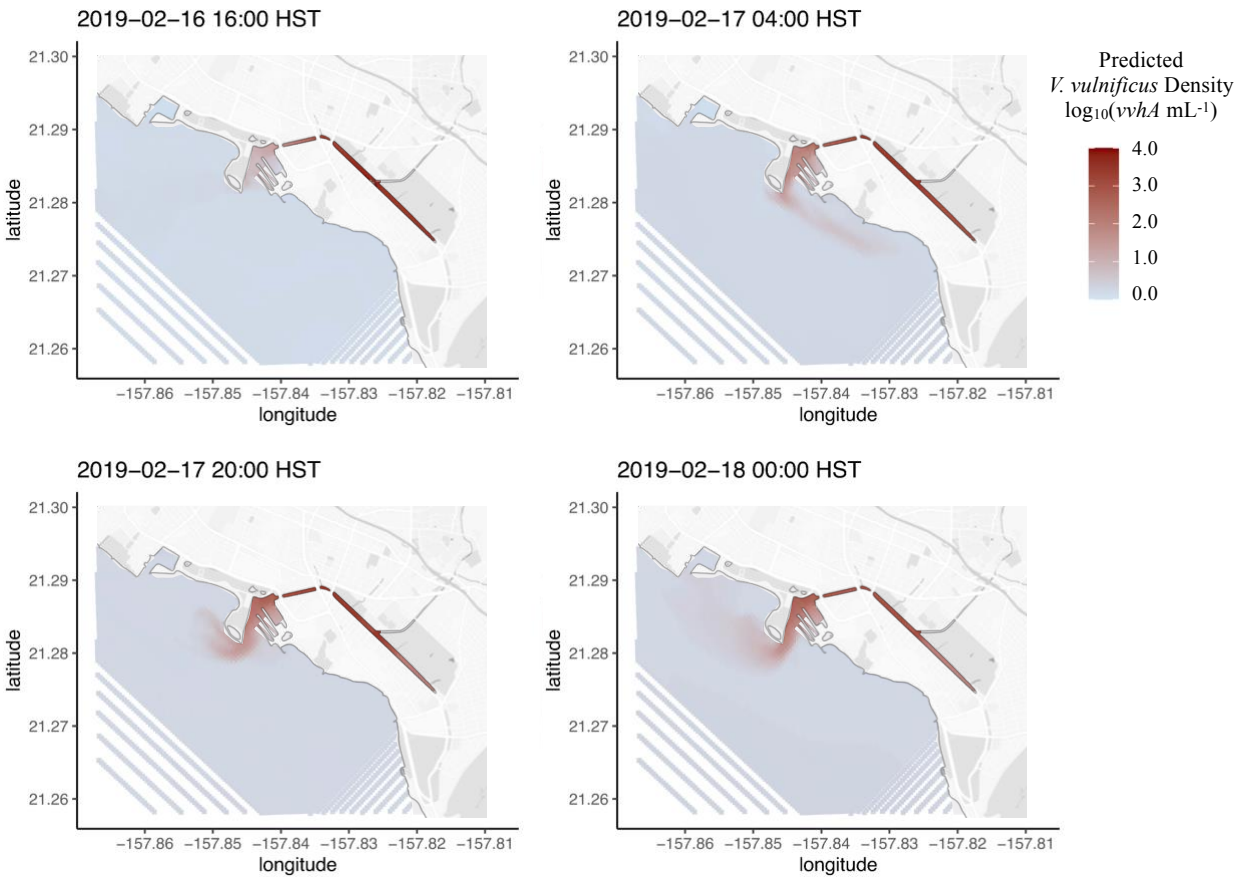

Figure 1.9 Applied model predictions (Table 1.2, Model 4) using the PacIOOS turbidity plume forecast showing plume dynamics of *V. vulnificus* density into recreational areas during a rain event (16-18 of February 2019).

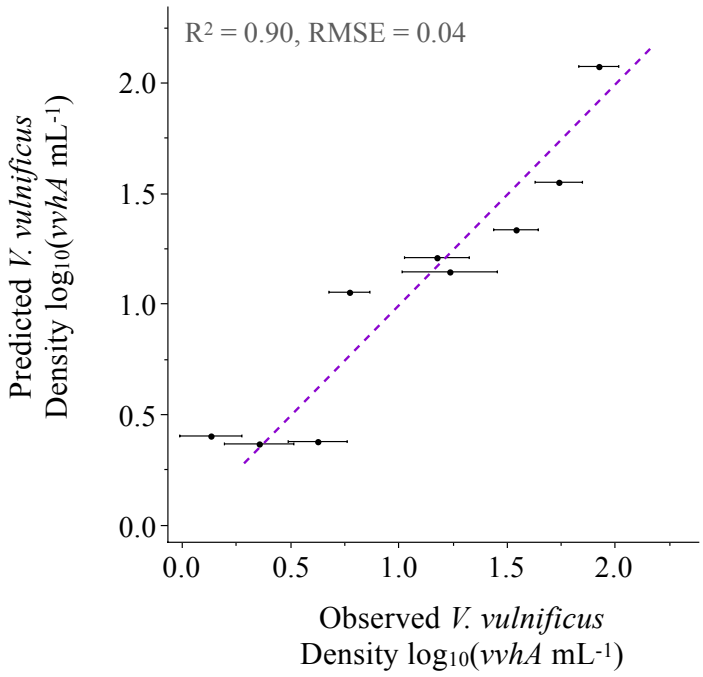

Figure 1.10 Climate-modeled *V. vulnificus* density based on rainfall and air temperature versus measured *V. vulnificus* density within the canal (sites 2-8). Measured *V. vulnificus* density is shown as the geometric mean with standard error around the mean value. The linear fit (y = 1x - 3.55e-15) is practically 1:1 and the 95 % confidence interval is shown in purple. The climate model does not predict the spatial variation in *V. vulnificus* density (R^2 = 0.42, RMSE = 0.65, *PE = 4.47), but expertly predicts the overall monthly average of *V. vulnificus* density within the canal (R^2 = 0.90, RMSE = 0.04, *PE = 1.1). Model coefficients were used to predict the long-term effects of changing rainfall and air temperature on overall average *V. vulnificus* density for the canal (see Figure 1.10). Model: $\log_{10}(vvhA) = 0.4414 * \log_{10}(\text{five-day average rainfall}) + 0.1405 * (\text{air temperature}) - 3.7750$

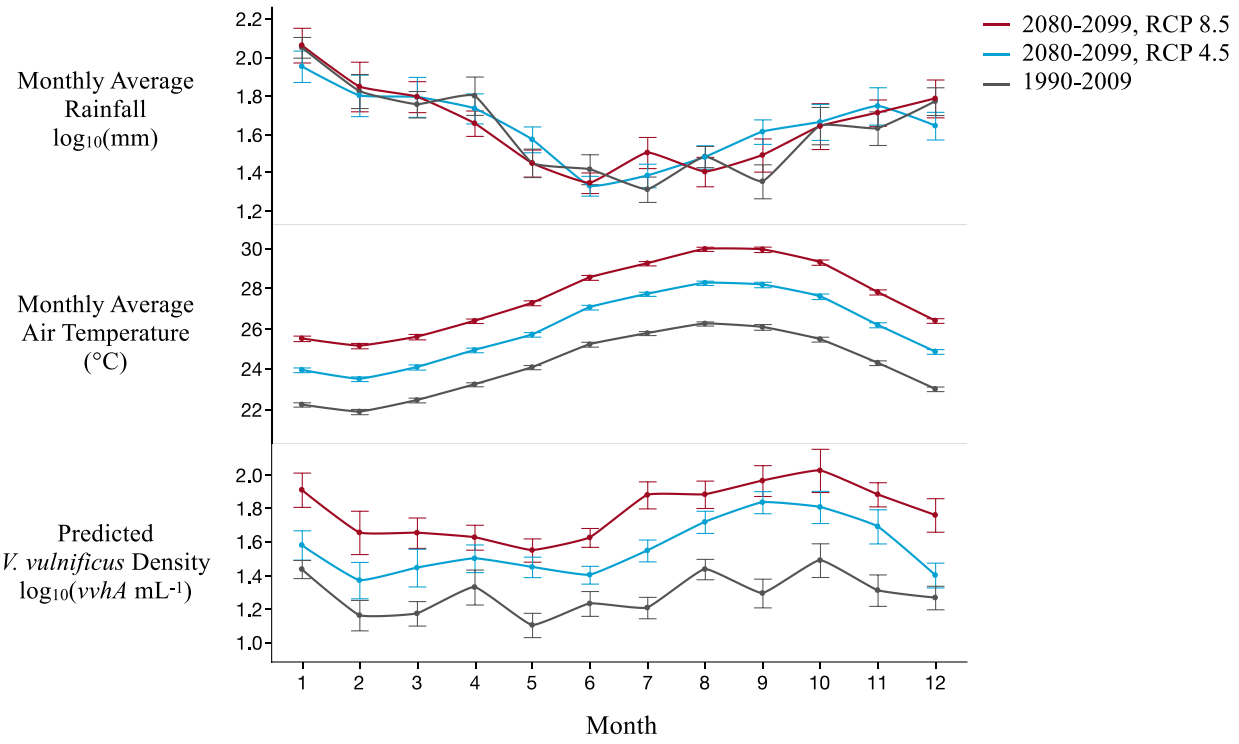

Figure 1.11 Monthly average climate projections of rainfall and air temperature based on dynamical downscaling (250 m resolution) of recorded data (1990-2009) and the AR5 RCP 4.5 and RCP 8.5 modeled scenarios* (2080-2099). Monthly average *V. vulnificus* density for the canal is predicted from rainfall and air temperature. Geometric mean values are shown with standard error around the mean value. There is no significant difference ($p = 0.45$) in annual average rainfall between the three projections (1990-2009, RCP 4.5, and RCP 8.5). There is a significant difference ($p < 0.0001$) in annual average air temperature and in *V. vulnificus* density between the three projections. Mean comparisons using Tukey-Kramer HSD show that RCP 8.5 (mean = 27.6 °C, 61.0 *vvhA* gene copies mL^{-1}) is significantly higher ($p < 0.0001$) than RCP 4.5 (mean = 26.0 °C, 36.5 *vvhA* gene copies mL^{-1}) and RCP 4.5 is significantly higher ($p < 0.0001$) than 1990-2009 (mean = 24.2 °C, 19.3 *vvhA* gene copies mL^{-1}).

*The Intergovernmental Panel on Climate Change (IPCC) 5th Assessment Report 2014. Representative Concentration Pathways. RCP 4.5: 580-720 ppm CO_2-eq by 2100 and 1.7-3.2 °C increase relative to 1850-1900. RCP 8.5: >1000 ppm CO_2-eq by 2100 and 3.2-5.4 °C increase relative to 1850-1900.

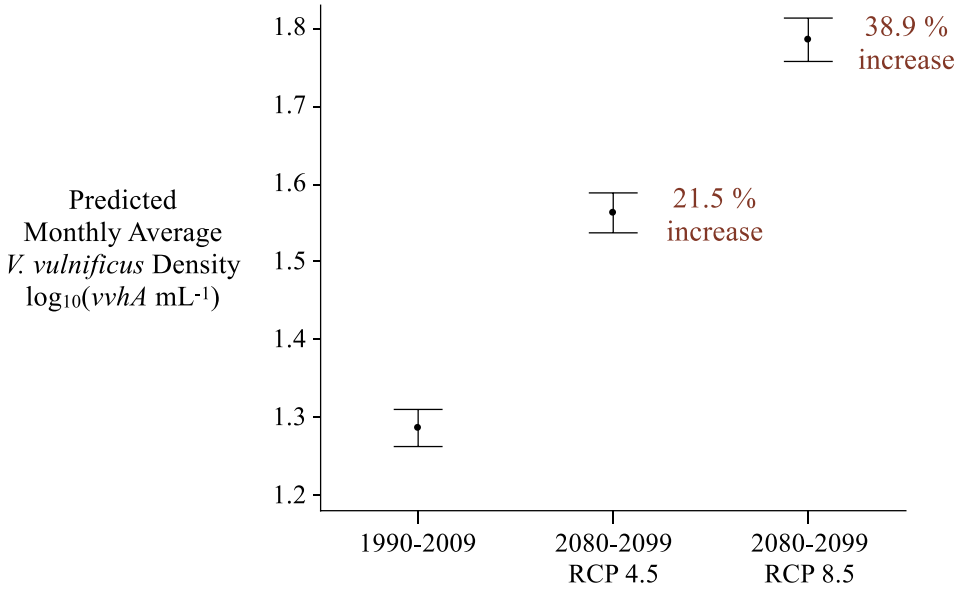

Figure 1.12 Predicted monthly average *V. vulnificus* density from climate projections of rainfall and air temperature based on dynamical downscaling (250 m resolution) of recorded data (1990-2009) and the AR5 RCP 4.5 and RCP 8.5 modeled scenarios (2080-2099). There is a significant difference ($p < 0.0001$) in predicted annual average *V. vulnificus* density between the three projections. Mean comparisons using Tukey-Kramer HSD show that RCP 8.5 (mean = 61.0 *vvhA* gene copies mL^{-1}) is significantly higher ($p < 0.0001$) than RCP 4.5 (mean = 36.5 *vvhA* gene copies mL^{-1}) and RCP 4.5 is significantly higher ($p < 0.0001$) than 1990-2009 (mean = 19.3 *vvhA* gene copies mL^{-1}). RCP 4.5 is a 21.5 % increase in *V. vulnificus* density relative to 1990-2009. RCP 8.5 is a 38.9 % increase in *V. vulnificus* density relative to 1990-2009.

1.8 ACKNOWLEDGEMENTS

I thank my coauthors, Abigail Golder, Grieg Steward, Margaret McManus, Anna Neuheimer, Brian Glazer, Olivia Nigro, and Craig Nelson, for their generous contributions to my thesis project and manuscript preparation. I also thank the many technicians, interns, and volunteers who assisted with collection of samples from the canal: Stanley Lio, Solomon Chen, Shaun Wriston, Han Quach, Eleanor Yuan, Wesley Sparagon, Rayna McClintock, Brenna Carroll, Sarah Michal Hamid, Brianna Ornelas, Seraphina King, Justin Higa, Cory Yap, Sarah Cory, Kira Webster, Alex Quiroz, Ashley Hi‘ilani Sanchez, Kyle Conner, Aka Beebe, Sean Mahaffey, Petra Byl, Cherise Spotkaeff, Isabelle Yazel, Nick Yoshioka, Kelsey Nichols, Zoe Glenn, Olivia Hughes, Maria Steadmon, Ashley Ostendorf, Sherine Boomla, and Sienna Santiago. I thank Danielle Hull who processed the nutrient samples at the SOEST Lab for Analytical Biogeochemistry, Kirsten Nakayama and Nicole Yoneishi who assisted with DNA extractions at the Microbial Genomics and Analytical Lab, and Abby Frazier who assisted with accessing the downscaled climate change projections. I thank PacIOOS and Gordon Walker for providing and maintaining real time data at NS02 and Brian Powell for creating and maintaining the turbidity plume model forecast. This project was funded by NOAA Sea Grant and the University of Hawai‘i at Mānoa Strategic Monitoring and Resilience Training in the Ala Wai.

1.9 LITERATURE CITED

Akaike H. (1973). Information Theory and an Extension of the Maximum Likelihood Principle. In: Parzen E., Tanabe K., Kitagawa G. (eds) Selected Papers of Hirotugu Akaike. *Springer Series in Statistics (Perspectives in Statistics)*, 199–213. https://doi.org/10.1007/978-1-4612-1694-0_15

Armstrong, F. A. J., Stearns, C. R., & Strickland, J. D. H. (1967). The measurement of upwelling and subsequent biological process by means of the Technicon Autoanalyzer® and associated equipment. *Deep-Sea Research and Oceanographic Abstracts*, *14*(3), 381–389. https://doi.org/10.1016/0011-7471(67)90082-4

Baker-Austin, C., Oliver, J. D., Alam, M., Ali, A., Waldor, M. K., Qadri, F., & Martinez-Urtaza, J. (2018). *Vibrio* spp. infections. *Nature Reviews Disease Primers*, *4*(1), 1–19. https://doi.org/10.1038/s41572-018-0005-8

Baker-Austin, C., Trinanes, J. A., Taylor, N. G. H., Hartnell, R., Siitonen, A., & Martinez-Urtaza, J. (2013). Emerging *Vibrio* risk at high latitudes in response to ocean warming. *Nature Climate Change*, *3*(1), 73–77. https://doi.org/10.1038/nclimate1628

Baker-Austin, C., Trinanes, J., Gonzalez-Escalona, N., & Martinez-Urtaza, J. (2017). Non-Cholera Vibrios: The Microbial Barometer of Climate Change. *Trends in Microbiology*, Vol. 25, pp. 76–84. https://doi.org/10.1016/j.tim.2016.09.008

Bartoń, K. (2019). MuMIn: Multi-Model Inference. R package version 1.43.6. https://CRAN.R-project.org/package=MuMIn

Belzile, C., Roesler, C. S., Christensen, J. P., Shakhova, N., & Semiletov, I. (2006). Fluorescence measured using the WETStar DOM fluorometer as a proxy for dissolved matter absorption. *Estuarine, Coastal and Shelf Science*, *67*(3), 441–449. https://doi.org/10.1016/j.ecss.2005.11.032

Bowers, D. G., & Brett, H. L. (2008). The relationship between CDOM and salinity in estuaries: An analytical and graphical solution. *Journal of Marine Systems*, *73*(1–2), 1–7. https://doi.org/10.1016/j.jmarsys.2007.07.001

Bustin, S. A., Benes, V., Garson, J. A., Hellemans, J., Huggett, J., Kubista, M., Mueller, R., Nolan, T., Pfaffl, M. W., Shipley, G. L., Vandesompele, J., & Wittwer, C. T. (2009). The MIQE Guidelines: Minimum Information for Publication of Quantitative Real-Time PCR Experiments. *Clinical Chemistry*, *55*(4), 611–622. https://doi.org/10.1373/clinchem.2008.112797

Cai, W. J. (2011). Estuarine and coastal ocean carbon paradox: CO_2 sinks or sites of terrestrial carbon incineration? *Annual Review of Marine Science*, *3*, 123–145. https://doi.org/10.1146/annurev-marine-120709-142723

Campbell, M. S., & Wright, A. C. (2003). Real-Time PCR Analysis of *Vibrio vulnificus* from

Oysters. *Applied and Environmental Microbiology*, *69*(12), 7137–7144. https://doi.org/10.1128/AEM.69.12.7137-7144.2003

Carstea, E. M., Popa, C. L., Baker, A., & Bridgeman, J. (2020). In situ fluorescence measurements of dissolved organic matter: A review. *Science of the Total Environment*, *699*, 134361. https://doi.org/10.1016/j.scitotenv.2019.134361

Chen, C. Y., Wu, K. M., Chang, Y. C., Chang, C. H., Tsai, H. C., Liao, T. L., Liu, Y. M., Chen, H. J., Shen, A. B. T., Li, J. C., Su, T. L., Shao, C. P., Lee, C. T., & Tsai, S. F. (2003). Comparative genome analysis of *Vibrio vulnificus*, a marine pathogen. *Genome Research*, *13*(12), 2577–2587. https://doi.org/10.1101/gr.1295503

Coble, P. G. (1996). Characterization of marine and terrestrial DOM in seawater using excitation-emission matrix spectroscopy. *Marine Chemistry*, *51*(4), 325–346. https://doi.org/10.1016/0304-4203(95)00062-3

Connolly, J. P., Blumberg, A. F., & Quadrini, J. D. (1999). Modeling the fate of pathogenic organisms in coastal waters of Oahu, Hawaii. *Journal of Environmental Engineering*, *125*(5), 398–406. https://doi.org/10.1061/(asce)0733-9372(1999)125:5(398)

De Carlo, E. H., Hoover, D. J., Young, C. W., Hoover, R. S., & Mackenzie, F. T. (2007). Impact of storm runoff from tropical watersheds on coastal water quality and productivity. *Applied Geochemistry*, *22*(8 SPEC. ISS.), 1777–1797. https://doi.org/10.1016/j.apgeochem.2007.03.034

DePaola, A., Capers, G. M., & Alexander, D. (1994). Densities of *Vibrio vulnificus* in the intestines of fish from the U.S. Gulf Coast. *Applied and Environmental Microbiology*, *60*(3), 984–988. https://doi.org/10.1128/aem.60.3.984-988.1994

Fiedler, J. W., McManus, M. A., Tomlinson, M. S., De Carlo, E. H., Pawlak, G. R., Steward, G. F., Nigro, O. D., Timmerman, R. E., Drupp, P. S., & Ostrander, C. E. (2014). Real-time observations of the February 2010 Chile and March 2011 Japan tsunamis recorded in Honolulu by the Pacific Islands Ocean Observing System. *Oceanography*, *27*(2), 186–200. https://doi.org/10.5670/oceanog.2014.34

Ghosh, A., & Bhadury, P. (2019). Exploring biogeographic patterns of bacterioplankton communities across global estuaries. *MicrobiologyOpen*, *8*(5), 741. https://doi.org/10.1002/mbo3.741

Givens, C. E., Bowers, J. C., Depaola, A., Hollibaugh, J. T., & Jones, J. L. (2014). Occurrence and distribution of *Vibrio vulnificus* and *Vibrio parahaemolyticus* - potential roles for fish, oyster, sediment and water. *Letters in Applied Microbiology*, *58*(6), 503–510. https://doi.org/10.1111/lam.12226

Gordon, D. G. (1969). Examination of methods of particulate organic carbon analysis. *Deep-Sea Research and Oceanographic Abstracts*, *16*(6), 661–665. https://doi.org/10.1016/0011-7471(69)90066-7

Grasshoff, K., Kremling, K., & Ehrhardt, M. (1983). Methods of seawater analysis. *Marine Chemistry*, *7*(1), 86–87. https://doi.org/10.1016/0304-4203(78)90045-2

Heng, S. P., Letchumanan, V., Deng, C. Y., Ab Mutalib, N. S., Khan, T. M., Chuah, L. H., Chan, K. G., Goh, B. H., Pusparajah, P., & Lee, L. H. (2017, May 31). *Vibrio vulnificus*: An environmental and clinical burden. *Frontiers in Microbiology*, *8*, 997. https://doi.org/10.3389/fmicb.2017.00997

Holland, P. M., Abramson, R. D., Watson, R., & Gelfand, D. H. (1991). Detection of specific polymerase chain reaction product by utilizing the 5′ → 3′ exonuclease activity of *Thermus aquaticus* DNA polymerase. *Proceedings of the National Academy of Sciences of the United States of America*, *88*(16), 7276–7280. https://doi.org/10.1073/pnas.88.16.7276

Horseman, M. A., & Surani, S. (2011). A comprehensive review of *Vibrio vulnificus*: An important cause of severe sepsis and skin and soft-tissue infection. *International Journal of Infectious Diseases*, *15*(3), e157-e166. https://doi.org/10.1016/j.ijid.2010.11.003

Huang, K. C., Weng, H. H., Yang, T. Y., Chang, T. S., Huang, T. W., & Lee, M. S. (2016). Distribution of fatal *Vibrio vulnificus* necrotizing skin and soft-tissue infections a systematic review and meta-analysis. *Medicine*, *95*(5). https://doi.org/10.1097/MD.0000000000002627

Huehn, S., Eichhorn, C., Urmersbach, S., Breidenbach, J., Bechlars, S., Bier, N., Alter, T., Bartelt, E., Frank, C., Oberheitmann, B., Gunzer, F., Brennholt, N., Böer, S., Appel, B., Dieckmann, R., & Strauch, E. (2014). Pathogenic vibrios in environmental, seafood and clinical sources in Germany. *International Journal of Medical Microbiology*, *304*(7), 843-850. https://doi.org/10.1016/j.ijmm.2014.07.010

IPCC (2014). Climate Change 2014: Synthesis Report. Contribution of Working Groups I, II and III to the Fifth Assessment Report of the Intergovernmental Panel on Climate Change [Core Writing Team, R.K. Pachauri and L.A. Meyer (eds.)]. IPCC, Geneva, Switzerland, 151. https://www.ipcc.ch/site/assets/uploads/2018/05/SYR_AR5_FINAL_full_wcover.pdf

Jacobs, J. M., Rhodes, M., Brown, C. W., Hood, R. R., Leight, A., Long, W., & Wood, R. (2014). Modeling and forecasting the distribution of *Vibrio vulnificus* in Chesapeake Bay. *Journal of Applied Microbiology*, *117*(5), 1312–1327. https://doi.org/10.1111/jam.12624

Johnson, A. E., Powell, B. S., & Steward, G. F. (2013). Characterizing the effluence near Waikiki, Hawaii with a coupled biophysical model. *Continental Shelf Research*, *54*, 1–13. https://doi.org/10.1016/j.csr.2012.12.007

Johnson, C. N., Flowers, A. R., Noriea, N. F., Zimmerman, A. M., Bowers, J. C., DePaola, A., & Grimes, D. J. (2010). Relationships between environmental factors and pathogenic vibrios in the northern gulf of Mexico. *Applied and Environmental Microbiology*, *76*(21), 7076–7084. https://doi.org/10.1128/AEM.00697-10

Johnson, K. S., & Coletti, L. J. (2002). In situ ultraviolet spectrophotometry for high resolution

and long-term monitoring of nitrate, bromide and bisulfide in the ocean. *Deep-Sea Research Part I: Oceanographic Research Papers*, *49*(7), 1291–1305. https://doi.org/10.1016/S0967-0637(02)00020-1

Jones, M. K., & Oliver, J. D. (2009). *Vibrio vulnificus*: Disease and pathogenesis. *Infection and Immunity*, *77*(5), 1723-1733. https://doi.org/10.1128/IAI.01046-08

Kan, J., Suzuki, M. T., Wang, K., Evans, S. E., & Chen, F. (2007). High temporal but low spatial heterogeneity of bacterioplankton in the Chesapeake Bay. *Applied and Environmental Microbiology*, *73*(21), 6776–6789. https://doi.org/10.1128/AEM.00541-07

Kaspar, C. W., & Tamplin, M. L. (1993). Effects of temperature and salinity on the survival of *Vibrio vulnificus* in seawater and shellfish. *Applied and Environmental Microbiology*, *59*(8), 2425–2429. https://doi.org/10.1128/aem.59.8.2425-2429.1993

Kérouel, R., & Aminot, A. (1997). Fluorometric determination of ammonia in sea and estuarine waters by direct segmented flow analysis. *Marine Chemistry*, *57*(3–4), 265–275. https://doi.org/10.1016/S0304-4203(97)00040-6

Lipp, E. K., Rodriguez-Palacios, C., & Rose, J. B. (2001). Occurrence and distribution of the human pathogen *Vibrio vulnificus* in a subtropical Gulf of Mexico estuary. In *The Ecology and Etiology of Newly Emerging Marine Diseases*, 165–173. https://doi.org/10.1007/978-94-017-3284-0_15

Martinez-Urtaza, J., Bowers, J. C., Trinanes, J., & DePaola, A. (2010). Climate anomalies and the increasing risk of *Vibrio parahaemolyticus* and *Vibrio vulnificus* illnesses. *Food Research International*, *43*(7), 1780–1790. https://doi.org/10.1016/j.foodres.2010.04.001

Maugeri, T. L., Carbone, M., Fera, M. T., & Gugliandolo, C. (2006). Detection and differentiation of *Vibrio vulnificus* in seawater and plankton of a coastal zone of the Mediterranean Sea. *Research in Microbiology*, *157*(2), 194–200. https://doi.org/10.1016/j.resmic.2005.06.007

McKinney, W. (2011). pandas: a Foundational Python Library for Data Analysis and Statistics. *Python for High Performance and Scientific Computing*, 1–9. Retrieved from https://www.dlr.de/sc/portaldata/15/resources/dokumente/pyhpc2011/submissions/pyhpc2011_submission_9.pdf

McManus, M.A. (2008), updated 2016. *PacIOOS Nearshore Sensor 02 (NS02): Hawaii Yacht Club, Oahu, Hawaii.* [1 October 2018 – 1 October 2019.] Distributed by the Pacific Islands Ocean Observing System (PacIOOS). http://pacioos.org/metadata/NS02agg.html. Accessed 16 December 2019.

Motes, M. L., DePaola, A., Cook, D. W., Veazey, J. E., Hunsucker, J. C., Garthright, W. E., Blodgett, R. J., & Chirtel, S. J. (1998). Influence of water temperature and salinity on *Vibrio vulnificus* in Northern Gulf and Atlantic Coast oysters (*Crassostrea virginica*). *Applied and Environmental Microbiology*, *64*(4), 1459–1465.

https://doi.org/10.1128/aem.64.4.1459-1465.1998

Muhling, B. A., Jacobs, J., Stock, C. A., Gaitan, C. F., & Saba, V. S. (2017). Projections of the future occurrence, distribution, and seasonality of three *Vibrio* species in the Chesapeake Bay under a high-emission climate change scenario. *GeoHealth*, *1*(7), 278–296. https://doi.org/10.1002/2017GH000089

Murphy, J., & Riley, J. P. (1962). A modified single solution method for the determination of phosphate in natural waters. *Analytica Chimica Acta*, *27*(C), 31–36. https://doi.org/10.1016/S0003-2670(00)88444-5

National Center for Emerging, C., & Infectious Diseases, Z. (2014). *National Enteric Disease Surveillance: COVIS Annual Summary*. https://www.cdc.gov/vibrio/surveillance.html

Nelson, C. E., Donahue, M. J., Dulaiova, H., Goldberg, S. J., La Valle, F. F., Lubarsky, K., Miyano, J., Richardson, C., Silbiger, N. J., & Thomas, F. I. M. (2015). Fluorescent dissolved organic matter as a multivariate biogeochemical tracer of submarine groundwater discharge in coral reef ecosystems. *Marine Chemistry*, *177*, 232–243. https://doi.org/10.1016/j.marchem.2015.06.026

Nelson, N. B., & Siegel, D. A. (2013). The global distribution and dynamics of chromophoric dissolved organic matter. *Annual Review of Marine Science*, *5*, 447–476. https://doi.org/10.1146/annurev-marine-120710-100751

Newton, A., Kendall, M., Vugia, D. J., Henao, O. L., & Mahon, B. E. (2012). Increasing rates of vibriosis in the United States, 1996-2010: Review of surveillance data from 2 systems. *Clinical Infectious Diseases*, *54*, 391–395. https://doi.org/10.1093/cid/cis243

Nigro, O. D. (2012). Environmental controls on *Vibrio vulnificus* and other pathogenic vibrios in tropical and subtropical coastal waters. *ProQuest Dissertations Publishing*. Retrieved from https://scholarspace.manoa.hawaii.edu/handle/10125/101007

Nigro, O. D., & Steward, G. F. (2015). Differential specificity of selective culture media for enumeration of pathogenic vibrios: Advantages and limitations of multi-plating methods. *Journal of Microbiological Methods*, *111*, 24–30. https://doi.org/10.1016/j.mimet.2015.01.014

Nuss, E. (2016). Predicting pathogenic bacteria concentrations with a coupled microbial-physical model. *ProQuest Dissertations Publishing*. Retrieved from https://www.soest.hawaii.edu/oceanography/masters/2016-Nuss.pdf

O'Neill, K. R., Jones, S. H., & Grimes, D. J. (1992). Seasonal incidence of *Vibrio vulnificus* in the Great Bay estuary of New Hampshire and Maine. *Applied and Environmental Microbiology*, *58*(10), 3257–3262. https://doi.org/10.1128/aem.58.10.3257-3262.1992

Paz, S., Bisharat, N., Paz, E., Kidar, O., & Cohen, D. (2007). Climate change and the emergence of *Vibrio vulnificus* disease in Israel. *Environmental Research*, *103*(3), 390–396.

https://doi.org/10.1016/j.envres.2006.07.002

Pfaffl, M. W. (2001). A new mathematical model for relative quantification in real-time RT–PCR. *Nucleic Acids Research*, *29*(9), E45. https://doi.org/10.1093/nar/29.9.e45

Pfeffer, C. S., Hite, M. F., & Oliver, J. D. (2003). Ecology of *Vibrio vulnificus* in estuarine waters of eastern North Carolina. *Applied and Environmental Microbiology*, *69*(6), 3526–3531. https://doi.org/10.1128/AEM.69.6.3526-3531.2003

Python Core Team (2015). Python: A dynamic, open source programming language. Python Software Foundation. URL https://www.python.org/

R Core Team (2019). R: A language and environment for statistical computing. R Foundation for Statistical Computing, Vienna, Austria. URL https://www.R-project.org/

Ralston, E. P., Kite-Powell, H., & Beet, A. (2011). An estimate of the cost of acute health effects from food- and water-borne marine pathogens and toxins in the USA. *Journal of Water and Health*, *9*(4), 680–694. https://doi.org/10.2166/wh.2011.157

Randa, M. A., Polz, M. F., & Lim, E. (2004). Effects of temperature and salinity on *Vibrio vulnificus* population dynamics as assessed by quantitative PCR. *Applied and Environmental Microbiology*, *70*(9), 5469–5476. https://doi.org/10.1128/AEM.70.9.5469-5476.2004

Ruhala, S. S., & Zarnetske, J. P. (2017). Using in-situ optical sensors to study dissolved organic carbon dynamics of streams and watersheds: A review. *Science of the Total Environment*, *575*, 713–723. https://doi.org/10.1016/j.scitotenv.2016.09.113

Sharp, J. H. (1974). Improved analysis for "particulate" organic carbon and nitrogen from seawater. *Limnology and Oceanography*, *19*, 984–989. https://doi.org/10.4319/lo.1974.19.6.0984

Shiller, A. M. (1996). The effect of recycling traps and upwelling on estuarine chemical flux estimates. *Geochimica et Cosmochimica Acta*, *60*(17), 3177–3185. https://doi.org/10.1016/0016-7037(96)00159-7

Smith, R. C, Baker, K. S, & Dustan, P. (1981). Fluorometric Techniques For The Measurement Of Oceanic Chlorophyll In The Support Of Remote Sensing. *UC San Diego: Library – Scripps Digital Collection*. Retrieved from https://escholarship.org/uc/item/4k51f7p0

Strom, M. S., & Paranjpye, R. N. (2000). Epidemiology and pathogenesis of *Vibrio vulnificus*. *Microbes and Infection*, *2*, 177–188. https://doi.org/10.1016/S1286-4579(00)00270-7

Tamplin, M., Rodrick, G. E., Blake, N. J., & Cuba, T. (1982). Isolation and characterization of *Vibrio vulnificus* from two florida estuaries. *Applied and Environmental Microbiology*, *44*(6), 1466–1470. https://doi.org/10.1128/aem.44.6.1466-1470.1982

Turner, J. W., Good, B., Cole, D., & Lipp, E. K. (2009). Plankton composition and environmental factors contribute to *Vibrio* seasonality. *ISME Journal*, *3*(9), 1082–1092. https://doi.org/10.1038/ismej.2009.50

Vezzulli, L., Brettar, I., Pezzati, E., Reid, P. C., Colwell, R. R., Höfle, M. G., & Pruzzo, C. (2012). Long-term effects of ocean warming on the prokaryotic community: Evidence from the vibrios. *ISME Journal*, *6*(1), 21–30. https://doi.org/10.1038/ismej.2011.89

Vezzulli, L., Colwell, R. R., & Pruzzo, C. (2013). Ocean Warming and Spread of Pathogenic Vibrios in the Aquatic Environment. *Microbial Ecology*, *65*(4), 817-825. https://doi.org/10.1007/s00248-012-0163-2

Vezzulli, L., Grande, C., Reid, P. C., Hélaouët, P., Edwards, M., Höfle, M. G., Brettar, I., Colwell, R. R., & Pruzzo, C. (2016). Climate influence on *Vibrio* and associated human diseases during the past half-century in the coastal North Atlantic. *Proceedings of the National Academy of Sciences of the United States of America*, *113*(34), E5062–E5071. https://doi.org/10.1073/pnas.1609157113

Wetz, J. J., Blackwood, A. D., Fries, J. S., Williams, Z. F., & Noble, R. T. (2013). Quantification of *Vibrio vulnificus* in an Estuarine Environment: a Multi-Year Analysis Using QPCR. *Estuaries and Coasts 2013 37:2*, *37*(2), 421–435. https://doi.org/10.1007/S12237-013-9682-4

Wright, A. C., Hill, R. T., Johnson, J. A., Roghman, M. C., Colwell, R. R., & Morris, J. G. (1996). Distribution of *Vibrio vulnificus* in the Chesapeake Bay. *Applied and Environmental Microbiology*, *62*(2), 717–724. https://doi.org/10.1128/aem.62.2.717-724.1996

Zhang, C., Wang Dr., Y., Lauer, A., & Hamilton, K. (2012). Configuration and evaluation of the wrf model for the study of hawaiian regional climate. *Monthly Weather Review*, *140*(10), 3259–3277. https://doi.org/10.1175/MWR-D-11-00260.1

Zhang, C., Wang, Y., Hamilton, K., & Lauer, A. (2016a). Dynamical downscaling of the climate for the Hawaiian islands. Part II: Projection for the late twenty-first century. *Journal of Climate*, *29*(23), 8333–8354. https://doi.org/10.1175/JCLI-D-16-0038.1

Zhang, C., Wang, Y., Hamilton, K., & Lauer, A. (2016b). Dynamical downscaling of the climate for the Hawaiian islands. Part II: Projection for the late twenty-first century. *Journal of Climate*, *29*(23), 8333–8354. https://doi.org/10.1175/JCLI-D-16-0038.1

CHAPTER 2

A comparison of experimental techniques for capturing the elusive mortality rate dynamics of *Vibrio vulnificus* in the Ala Wai Canal

Keywords*: Vibrio vulnificus*, Pathogen, Estuary, Hawai‘i, Dilution Experiment, Eukaryotic Inhibition, Grazer, Viral Lysis, Mortality Rate

2.1 ABSTRACT

Mortality is an essential aspect of population control with different dynamics than those governing growth. In order to construct mechanistic models of populations over time, a mortality term is required and is often poorly constrained. Direct measurements of mortality, especially for microbial communities, is reasonably difficult. Several techniques have been developed to assess mortality rates of natural microbial populations. With varying degrees of success, these techniques have been applied to phytoplankton and more recently heterotrophic bacteria including the pathogenic *Vibrio cholerae*. Identifying and incorporating constraints on mortality rates of *Vibrio vulnificus* would likely benefit predictive modeling capabilities. I tested two techniques on *V. vulnificus* from the Ala Wai Canal in Honolulu, Hawai‘i. The dilution method systematically reduces grazing pressure in order to measure the impact of predation on mortality rate. I modified the dilution method to assess both grazing and viral lysis. In addition, I tested a eukaryotic inhibitor to compare and validate the grazing dilution method. In most cases, there was not a significant difference between the control and test treatments and there was large variation in responses between replicates. However, overall, the more diluted treatments grew faster suggesting a positive response to the removal of predators and viruses. The gross growth rates of the dilution experiments were ultimately closer than the inhibition experiment to the gross growth rates expected based on the multifactorial growth experiment (~0.6 h^{-1} based on a salinity of 11.19 and 24.57 °C). Mortality rates were comparable to gross growth rates (~0.2 –

0.7 h^{-1}) suggesting that natural population growth is limited by grazing and viral lysis. Natural populations of *V. vulnificus* may remain constant even with abundant resources due to tightly coupled growth with grazing and viral lysis.

2.2 INTRODUCTION

Numerical Population Modeling of **Vibrio vulnificus** *in the Ala Wai Canal*

In addition to statistical correlation modeling, efforts have been made to construct a mechanistic numerical population model for *Vibrio vulnificus* in the Ala Wai Canal (Nuss, 2016). The importance of salinity and temperature on *V. vulnificus* growth have been well documented (Motes et al., 1998; Jones and Oliver, 2009; Huehn et al., 2014; Kaspar and Tamplin 1993; Randa et al., 2004). Using a *V. vulnificus* isolate from the Ala Wai Canal, growth rates have been constrained over salinity (0 – 36) and temperature (24 – 36 °C) using multifactorial experiments (Figure 2.1; Steward and Nigro, unpublished). Based on these laboratory experiments of *V. vulnificus* growth, Nuss (2016) constructed a coupled physical-microbial numerical model of *V. vulnificus* population dynamics in the Ala Wai Canal. Their microbial model (Nuss, 2016; equation 2.1) incorporates growth based on the constraints of salinity and temperature. However, the mortality term is assumed to be constant and linearly scaled by the ratio of current *V. vulnificus* abundance to lagged abundance to account for the increase in mortality as the population grows, as well as depth to account for the increase in mortality in marine waters. Model results of *V. vulnificus* abundance are significantly different than observations from November 2008 – March 2009 for the three regions evaluated (the back end of the canal, the elbow where the canal bends towards the ocean, and the Ala Wai Harbor). Therefore, dynamic mortality rates may be more appropriate and improve model results.

Techniques to Assess Mortality Rate

I tested two methods of capturing *in situ* mortality rates with whole water (unamended) manipulations and incubations. The first method that is a eukaryotic inhibition with cytochalasin B. The second method is the dilution experiment which was developed by Landry and Hassett (1982). Both methods operate by systematically removing predators and/or viruses, releasing predation pressure and thereby promoting growth of the organism of interest. The change in growth rate is interpreted as the mortality rate. The dilution experiment technique is to serially dilute whole water with filtered water to linearly remove predation pressure. The resulting linear increase in growth rate with dilution is interpreted as the mortality rate (Figure 2.2). It was

originally developed for eukaryotic phytoplankton and grazers (Landry and Hassett, 1982) and later modified for prokaryotic phytoplankton (Worden and Binder, 2003) and heterotrophic prokaryotes (Jacquet at al., 2005). Landry et al. (1995) modified the experimental design to include a nutrient enrichment at the start of the experiment in order to remove any potential for nutrient limitation derived from the dilution itself and the removal of predators as a source of nutrient recycling. The gross growth rate, interpreted as the intercept of the dilution-growth curve which corresponds to all predation pressure removed, is then corrected by the difference in growth rate between the unenriched and enriched whole water. Furthermore, Li et al. (2017) attempted to account for nonlinear responses in the dilution-growth curve using a Holling II feeding response which addresses grazing saturation. Grazing saturation would mean that the grazing capacity is exceeded in the whole water, so the initial dilutions (75 % whole water for instance) have no effect on the grazing rate and therefore no effect on the growth rate of the organism of interest. This creates a depression in the dilution-growth curve which can be modeled to extract a mortality rate (Li et al., 2017). A final modification was to include the "predation pressure" of viral lysis (Jacquet at al. 2005; Kimmance et al., 2007; Mojica et al., 2016; Tijdens et al., 2008). In this design, the diluent is ultrafiltered either at 30 kDa or 100 kDa to remove both grazers and viruses. The results are then compared to a parallel experiment with traditional 0.45 μm or 0.2 μm filtered diluent which removes only grazers in order to approximate the effect of viral lysis on mortality rate. Enrichment is necessary with the viral lysis dilution experiment because the 30 kDa or 100 kDa filtration removes nutrients and depresses phytoplankton growth through nutrient limitation (Kimmance et al., 2007).

Although the dilution experiment design has been used successfully for total heterotrophic prokaryotes (Jacquet et al., 2005; Tijdens et al., 2008), there are only a handful of studies which assess the mortality rate of specific bacteria species using the dilution experiment design. For one, Worden et al. (2006) evaluated the trophic regulation of *V. cholerae*. In this case, *V. cholerae* cells from particular strains were inoculated into whole water rather than tracking a natural population. The efficacy of using these techniques to track a single population in a natural community without inoculation has yet to be shown.

Project Objectives

In order to begin to constrain the mortality rates to improve the coupled physical circulation and microbial population model, I tested these methods on natural microbial communities with *V. vulnificus* from the Ala Wai Canal. *V. vulnificus* predators are thought to be mainly ciliates and nanoflagellates and infrequently other bacteria (Chen et al., 2011). Additional mortality of *V. vulnificus* is likely caused by bacteriophages. *V. vulnificus* bacteriophage VvAW1 was isolated from the Ala Wai Canal and described in Nigro et al. (2012). However, the absolute and relative contribution of predation and viral lysis to *V. vulnificus* mortality is unknown. The dynamics of mortality are also unknown. There are likely seasonal and biogeochemical controls on mortality which could be employed to improve the coupled physical-microbial model and assist predictions for early warnings of pathogen exposure risk in coastal waters. Here, I report the results of three experiments run simultaneously and suggestions for improvement in the future.

2.3 MATERIALS AND METHODS

Water Collection

Whole water was hand collected in three 20-L, acid-cleaned polypropylene carboys on February 18, 2019 at 11:50 from the back end of the canal (21.275267° N, 157.8179596°W) at 0.25 m from the surface. *V. vulnificus* is consistently found at this location (see Chapter 1, Figure 1.3). The salinity was 11.19 and the water temperature was 24.57 °C.

Inhibition Experiment Design

Subsamples of whole water (400 mL) were transferred to 1-L, acid-cleaned flasks in triplicate. At 17:49 (six hours after water collection), 40 µL of cytochalasin B was added to each flask. The experiment was run in the lab at 20.5 °C in ambient lab lighting (overhead fluorescent lights). Samples were collected to analyze total prokaryote abundance and *V. vulnificus* abundance every hour for three hours beginning at 18:40 (T0) and ending at 21:41 (T3). Samples were collected using a peristaltic pump with acid-cleaned tubing kept inside the flasks for the entire experiment duration. Before sample collection, the flasks were mixed by hand and 20 mL was pumped from the flasks through the tubing with no filter attached to flush the lines. The cytochalasin B inhibition treatment was compared to the dilution experiment control samples (whole water with no organic enrichment; see *Grazing Mortality Dilution Experiment*) to calculate mortality rates.

Grazing Mortality Dilution Experiment

Five dilution treatments were applied to whole water incubations: 100 % whole water without tryptic soy broth (TSB) enrichment, 100 % whole water with TSB enrichment, 70 % whole water and 30 % diluent, 40 % whole water and 60 % diluent, and 20 % whole water and 80 % diluent. For the grazing-only experiment, the diluent was generated by filtering whole water into acid-cleaned, 20-L carboys using an in-line filter capsule (dual-layer 0.8 µm/ 0.2 µm polyethersulfone membrane; Whatman) and a peristaltic pump. Filtering began at 15:17 (roughly three hours after water collection) and intake was rotated among the three collection carboys every five minutes to effectively mix the source water. Filtered and whole water were combined

in correct proportions in 10-L polycarbonate carboys creating 7 L of the two whole water and three diluted treatments. At 17:50, 1.75 mL of TSB was added and mixed thoroughly into the 7L treatment carboys (~100 μM labile carbon), except the whole water without TSB treatment. Two liters from each treatment and control carboy was then transferred into triplicate 2-L polycarbonate bottles and then randomly arranged on a cart to begin the experiment.

In parallel with the inhibition experiment, the grazing dilution experiment was run in the lab at 20.5 °C in ambient lab lighting. Samples were collected to quantify concentrations of total prokaryotes and *V. vulnificus* every hour for three hours beginning at 18:40 (T0) and ending at 21:41 (T3). Samples were collected using a peristaltic pump with acid-cleaned intake tubing kept inside the bottles for the entire experiment duration. Before sample collection, the bottles were gently hand-mixed and 20 mL was pumped from the bottles with no filter attached to flush the tubing lines.

Grazing Plus Viral Mortality Dilution Experiment

This dilution experiment was run in tandem with the two previously described experiments. In this case, the diluent was ultrafiltered at 100 kDa to remove both grazers and viruses for the three dilution treatments (70 %, 40 %, and 20 % whole water). The 0.8 μm/ 0.2 μm filtrate was filtered using tangential flow ultrafiltration (100 kDa ultracel, Millipore) at 1.5 L min^{-1}. The effectiveness of the 0.2 μm and 100 kDa filtration was determined using epifluorescence microscopy to count cells and viruses before and after filtration. The 0.2 μm filtration removed 99 % of bacteria and kept 98 % of viruses. The 100 kDa filtration removed 100 % of bacteria and ~100 % of viruses. The remainder of the experiment was carried out as described above in the grazing-only dilution experiment. Whole water treatments were the same bottles as in the grazing only experiment.

Quantifying Microbial Abundance

Total Prokaryote Abundance

Total prokaryotic abundance was determined using an Attune Acoustic Focusing Cytometer according to Nelson et al. (2015) from whole water samples fixed with paraformaldehyde (0.5% final concentration) and stained with 1X SYBR Green I.

DNA Extraction Protocol

Samples for DNA extraction were collected by passing water through 0.22 µm polyethersulfone filters (Sterivex, Millipore); the exact filtrate volume was recorded (250-500 mL). Filters were added to MP Biomedicals Lysing Matrix A (No. 116910100) tubes with MC 1 lysis buffer and homogenized using a MP Biomedicals FastPrep-96 bead beater. DNA extractions were completed using the Macherey-Nagel NucleoMag Plant Extraction Kit (No. 744400.4) with KingFisher accessory kit (No. 744951). Samples were eluted to a final volume of 110 µL.

Quantifying Vibrio vulnificus

There is a consistent log correlation between CHROMagar *Vibrio* blue colony forming units and *vvhA* gene copy concentrations (Nigro & Steward, 2015). Therefore, I used a 16S rRNA 5' nuclease *vvhA* qPCR assay (Campbell & Wright, 2003; Holland et al., 1991; forward primer: 5'-TGTTTATGGTGAGAACGGTGACA-3'; reverse primer: 5'-TTCTTTATCTAGGCCCCAAACTTG-3'; 5'-Nuclease probe: 5'-/56-FAM/CCGTTAACC/ZEN/GAACCACCCGCAA/31ABkFQ/-3') to determine total *V. vulnificus* abundance. A 25 µL reaction mixture was prepared with final concentrations of 1X Kapa Probe Force Master Mix (Kapa Biosystems), 0.9 µM of each primer, 0.5 µM of the labeled probe, 0.56 mg/ml bovine serum albumin (Thermofisher), and 5 µL of DNA template (11.4 – 22.7 mL sample water). All qPCR reactions were performed in triplicate with the final replicate diluted 10-fold to check for inhibition of amplification as suggested by Bustin et al. (2009). The cycling protocol consisted of an initial denaturation step at 95 °C for 10 minutes, followed by 40 cycles of denaturation at 95 °C for 15 s and a combined annealing/extension at 60 °C for 30 minutes. I created an eight-point standard curve (10 – 50,000 copies per reaction well) of genomic DNA from *V. vulnificus* (strain YJ016; Chen et al., 2003) with known gene copy numbers per reaction run in triplicate along with the environmental samples. Assay efficiency was calculated from multiple standard curves using the formula $E = -1 + 10^{(-1/slope)}$ (Pfaffl, 2001).

Statistical Analysis

Linear least squares regression analyses in R version 3.1.6 (R Core Team, 2019) were

performed to calculate growth rates of total prokaryotes and *V. vulnificus* for each bottle replicate ("A, B, C") in the three experiments and across all replicates for each treatment ("R") according to the exponential growth rate formula, net growth rate (h^{-1}) = ln(concentration change) / time (h). To account for a possible lag, or acclimation, in the response of *V. vulnificus*, results were compared including and excluding the T0 time point. Growth rates for total prokaryotes were always lagged until the final time point, so growth calculations were based on changes in prokaryote concentrations between the third and final time point. Total prokaryotes also grew faster than *V. vulnificus* and are reported min^{-1}.

For the inhibition experiment, growth rate in the samples treated with cytochalasin B was interpreted as gross growth rate and growth rate in unamended, undiluted whole water was interpreted as net growth rate. An estimate of mortality rate was calculated as the difference between the two. For the dilution experiments, gross growth rate and mortality rate were calculated according to the following formula.

Net growth rate (h^{-1}) = – mortality rate (h^{-1}) * proportion whole water + gross growth rate (h^{-1})

2.4 RESULTS

Total Prokaryote Response

Inhibition Experiment

Total prokaryotes grew at an average of 0.384 cells mL^{-1} min^{-1} in the inhibition treatment and 0.634 cells mL^{-1} min^{-1} in the control (Figure 2.3). Prokaryote density peaked at the second time point (~1 h) for replicates A and B and at the third time point (~2 h) for replicate B in the inhibition treatments. Prokaryote density declined in the whole water control until the final time point. Net growth rate was calculated individually for the three replicates in each treatment. There was not a significant difference in the growth rates between the whole water control and the inhibition treatment ($p = 0.245$). The difference growth rates between treatment and control (Figure 2.3) defined a mortality rate of 0.250 cells mL^{-1} min^{-1}.

Grazing Only Dilution Experiment

Total prokaryotes in the grazer only dilution experiment grew only between the third and final time point (Figure 2.4) for all treatments. Individual growth rates per bottle varied from 0.1 to 0.6 cells mL^{-1} min^{-1}. Average growth rates were similar across all treatments, even the whole water without TSB, resulting in a dilution curve with a weak positive slope (Figure 2.5). Mortality and gross growth rates are interpreted as -0.10 cells mL^{-1} min^{-1} and 0.28 cells mL^{-1} min^{-1} respectively. However, a negative mortality term implies that the dilution had a negative effect on growth rather than stimulating growth, so the mortality rate is not interpretable.

Grazing and Viral Lysis Dilution Experiment

Similarly, in the grazing plus viral lysis dilution experiment, growth in total prokaryotes was only detected between the third and final time points (Figure 2.6). Individual growth rates per bottle varied from 0.1 to 0.8 cells mL^{-1} min^{-1}. The variance in growth rates of the replicates between treatments was substantial (see 20 % versus 40 % in Figure 2.6). Average growth rates were similar across all treatments, even the whole water without TSB, resulting in a dilution curve with a weak positive slope (Figure 2.7). Mortality and gross growth rates are interpreted as -0.17 cells mL^{-1} min^{-1} and 0.32 cells mL^{-1} min^{-1}, respectively.

Viral Lysis Contribution to Mortality

The contribution of viral lysis to total prokaryote mortality is the grazing plus viral lysis mortality rate minus the grazing only mortality rate. However, both mortality rates were negative which indicates a flaw in the experimental design, so a viral contribution could not be calculated.

Vibrio vulnificus *Response*

Inhibition Experiment

For the *V. vulnificus* analysis, I compared the growth rates calculated from the whole dataset to growth rates calculated without the initial T0 time point to account for an acclimation lag. For the full dataset, the inhibition treatment growth rate was 0.26 *vvhA* gene copies mL^{-1} h^{-1} ($R^2 = 0.29$) and there was a significant effect of time on concentration ($p < 0.001$; Figure 2.8). The whole water control growth rate was -0.08 gene copies mL^{-1} h^{-1} ($R^2 = 0.02$) with no significant effect of time on density ($p = 0.41$). The inhibition treatment net growth rate (0.26 *vvhA* gene copies mL^{-1} h^{-1}) is interpreted as the gross growth rate. The difference in inhibition treatment net growth rate and whole water net growth rate (0.34 *vvhA* gene copies mL^{-1} h^{-1}; Figure 2.8) is interpreted as the mortality rate. There was not a significant difference between the treatments ($p = 0.12$).

For the dataset without the initial T0 time point, the inhibition treatment growth rate was 0.21 *vvhA* gene copies mL^{-1} h^{-1} ($R^2 = 0.12$) and there was no significant effect of time on concentration ($p = 0.06$; Figure 2.8). The whole water control growth rate was 0.06 gene copies mL^{-1} h^{-1} ($R^2 = 0.01$) with no significant effect of time on density ($p = 0.68$). The inhibition treatment net growth rate (0.21 *vvhA* gene copies mL^{-1} h^{-1}) is interpreted as the gross growth rate. The difference in inhibition treatment net growth rate and whole water net growth rate (0.15 *vvhA* gene copies mL^{-1} h^{-1}) is interpreted as the mortality rate. There was not a significant difference between the treatments ($p = 0.28$).

Grazing Only Dilution Experiment

For the full dataset, growth rates ranged from -0.08 to 0.68 *vvhA* gene copies mL^{-1} h^{-1} across the treatments (Figure 2.9). All treatments, except the whole water without TSB, had a significant effect of time on density ($p < 0.05$) suggesting resolvable growth. The highest growth

rate (0.68 *vvhA* gene copies mL^{-1} h^{-1}) was detected in the 20 % whole water treatment as expected. From the dilution curve (Figure 2.10, top panel), the mortality rate is interpreted as 0.44 *vvhA* gene copies mL^{-1} h^{-1} and the gross growth rate is 0.59 *vvhA* gene copies mL^{-1} h^{-1}. There was a significant effect of dilution (proportion of whole water) on the net growth rates ($p < 0.05$) suggesting a resolvable dilution curve.

For the dataset without the initial T0 time point, growth rates ranged from 0.06 to 0.83 *vvhA* gene copies mL^{-1} h^{-1} across the treatments (Figure 2.9). All treatments, except the whole water without TSB, had a significant effect of time on density ($p < 0.05$) suggesting resolvable growth. The highest growth rate (0.83 *vvhA* gene copies mL^{-1} h^{-1}) was detected in the 40 % whole water treatment. From the dilution curve (Figure 2.10, bottom panel), the mortality rate is interpreted as 0.37 *vvhA* gene copies mL^{-1} h^{-1} and the gross growth rate is 0.76 *vvhA* gene copies mL^{-1} h^{-1}. There was not a significant effect of dilution (proportion of whole water) on the net growth rates ($p = 0.11$).

Grazing and Viral Lysis Dilution Experiment

For the full dataset, growth rates ranged from -0.08 to 0.57 *vvhA* gene copies mL^{-1} h^{-1} across the treatments (Figure 2.11). All treatments, except the whole water without TSB, had a significant effect of time on density ($P < 0.05$) suggesting resolvable growth. The highest growth rate (0.57 *vvhA* gene copies mL^{-1} h^{-1}) was detected in the 40 % whole water treatment. From the dilution curve (Figure 2.12, top panel), the mortality rate is interpreted as 0.26 *vvhA* gene copies mL^{-1} h^{-1} and the gross growth rate is 0.42 *vvhA* gene copies mL^{-1} h^{-1}. There was not a significant effect of dilution (proportion of whole water) on the net growth rates ($p = 0.38$).

For the dataset without the initial T0 time point, growth rates ranged from 0.06 to 1.02 *vvhA* gene copies mL^{-1} h^{-1} across the treatments (Figure 2.11). All treatments, except the whole water without TSB, had a significant effect of time on density ($P < 0.05$) suggesting resolvable growth. The highest growth rate (1.02 *vvhA* gene copies mL^{-1} h^{-1}) was detected in the 40 % whole water treatment. From the dilution curve (Figure 2.12, bottom panel), the mortality rate is interpreted as 0.73 *vvhA* gene copies mL^{-1} h^{-1} and the gross growth rate is 0.99 *vvhA* gene copies mL^{-1} h^{-1}. There was not a significant effect of dilution (proportion of whole water) on the net growth rates ($p = 0.18$).

Viral Lysis Contribution to Mortality

The contribution of viral lysis to total prokaryote mortality is the grazing plus viral lysis mortality rate minus the grazing only mortality rate. For the full dataset, the viral lysis mortality rate is -0.18 *vvhA* gene copies mL^{-1} h^{-1} which is not interpretable since the combined mortality rate was smaller than the mortality rate of grazing alone. For the dataset without T0, the viral lysis mortality rate is 0.36 *vvhA* gene copies mL^{-1} h^{-1}.

2.5 DISCUSSION

General Conclusions

Gross growth rates and mortality rates for all experiments are reported in Table 2.1. There are clearly different responses of the total prokaryote and *V. vulnificus* populations to the treatment manipulations. In the inhibition experiment, total prokaryote density peaked by the second time point (within 1 h). The total prokaryote density was stable or declining until the final time point in the dilution experiments, whereas the *V. vulnificus* population was reliably growing by the second time point for all treatments, even inhibition, except in the whole water without TSB. This result suggests that the whole water manipulations did have the growth stimulating effect that was expected by the experimental design for *V. vulnificus* density. In some cases, particularly when the T0 time point was removed, the 40 % whole water treatment had the highest growth rate which might suggest a saturation in gross growth rate before the most diluted treatment. However, overall, the more diluted treatments grew faster despite having an equivalent amount of TSB enrichment, suggesting a response to the removal of predators and/or viruses. There was also not a discernable nonlinear response in the dilution curve. The gross growth rates of the dilution experiments were ultimately closer than the inhibition experiment to the gross growth rates expected based on the multifactorial growth experiment (~0.6 h^{-1} based on a salinity of 11.19 and 24.57 °C, Figure 2.1). The lower rate for the inhibition experiment may have been a result of the lower temperature (20.5 °C) where the experiment was run in the lab.

A clear interpretation of these results is difficult to extract. The dilution may have unaccounted for effects, such as removing competitors which would stimulate growth and lead to an overestimation of mortality rate. In contrast, dilution may remove particles and nutrients not replaced by TSB enrichment which would depress or limit growth and lead to an underestimate of mortality rate.

Recommendations for Future Tests

There are several modifications to the experimental design which may improve our confidence in the mortality and gross growth rates. For one, this experiment was rather short (3 h duration) compared to the traditional 24 h for these experiments (Mojica et al., 2016; Worden

and Binder, 2003) or even longer incubations such as in Tijdens et al. (2008) who ran incubations for 40 h. A longer experiment duration might lead to a more distinguishable growth curve where the lag, or acclimation, period can be removed with more confidence. There was a clear lag in response by total prokaryotes. It is possible that the total prokaryote density was not changing for the first few time points because the relative abundance of populations within the community was changing and acclimating to the treatment before overall growth was resolvable. There was also a possible lag in response by *V. vulnificus* which motivated evaluation of the data without the initial time point. There was also a long period (~ 7 h) between water collection and the start of the experiment. It took ~ 4 h to prepare the different treatments which meant that the experiment was running in the light of the lab when it was naturally dark outside. The diel cycle of growth is notably important in the growth of microbes (Kelly et al., 2019; Ottesen et al., 2014). A smaller scale experiment with fewer treatments would accelerate the time to collect water, create the treatments, and begin the experiment. Performing the experiment in the field, possibly submerging the bottles *in situ* or at least running the experiment at *in situ* temperature, would likely reduce the time for acclimation. Finally, there is also a concerning amount of variation between the replicates in each treatment for *V. vulnificus* density despite our best efforts to aliquot the replicates immediately preceding the experiment. As in Worden et al. (2015), inoculation with *V. vulnificus* may be necessary in order to standardize the initial population abundance and inflate the natural low abundance population to reliably detectable levels with qPCR. However, this inoculation could change community interactions and affect results.

Ultimately, the variation in mortality rate across the physical and chemical environment of the canal is more important than the absolute rate numbers for modeling the population dynamics. A reliable sampling design with the fewest treatments possible, such as the inhibition experiment or a 2-point dilution experiment, with the fewest sampling times possible would allow for coverage of more locations and environmental conditions. Mortality rate as a function of temperature and salinity would complement the growth rate as a function of temperature and salinity to improve the existing physical-microbial model for real time predictions of *V. vulnificus* in the Ala Wai Canal.

2.6 TABLES

Table 2.1 Summary of mortality and gross growth rates from all three experiments. *V. vulnificus* data are separated into two datasets: the full dataset and the dataset without T0. The viral contribution to mortality is calculated for the *V. vulnificus* dilution curves without T0. It is not calculated for the total prokaryote or *V. vulnificus* full dataset dilution curves because the values are not interpretable.

Total prokaryotes	**Inhibition experiment**	**Grazing and viral lysis dilution experiment**	**Grazing only dilution experiment**	**Viral contribution**
Gross growth rate (cells mL^{-1} min^{-1})	0.38	0.32	0.28	NA
Mortality rate (cells mL^{-1} min^{-1})	0.25	-0.17	-0.10	NULL
***V. vulnificus* full dataset**	**Inhibition experiment**	**Grazing and viral lysis dilution experiment**	**Grazing only dilution experiment**	**Viral contribution**
Gross growth rate (*vvhA* copies mL^{-1} h^{-1})	0.26	0.42	0.59	NA
Mortality rate (*vvhA* gene mL^{-1} h^{-1})	0.34	0.26	0.44	NULL
***V. vulnificus* without T0**	**Inhibition experiment**	**Grazing and viral lysis dilution experiment**	**Grazing only dilution experiment**	**Viral contribution**
Gross growth rate (*vvhA* copies mL^{-1} h^{-1})	0.21	0.99	0.76	NA
Mortality rate (*vvhA* copies mL^{-1} h^{-1})	0.15	0.73	0.37	0.36

2.7 FIGURES

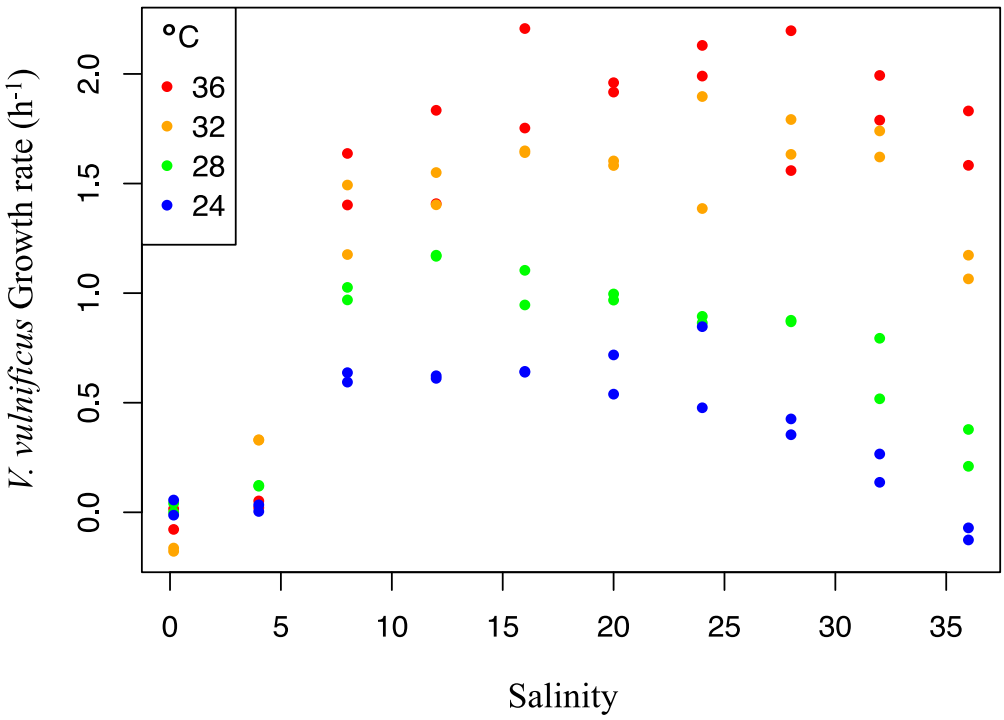

Figure 2.1 Laboratory growth rates of *Vibrio vulnificus* isolated from the Ala Wai Canal at various combinations of salinity and temperature (Steward and Nigro, unpublished).

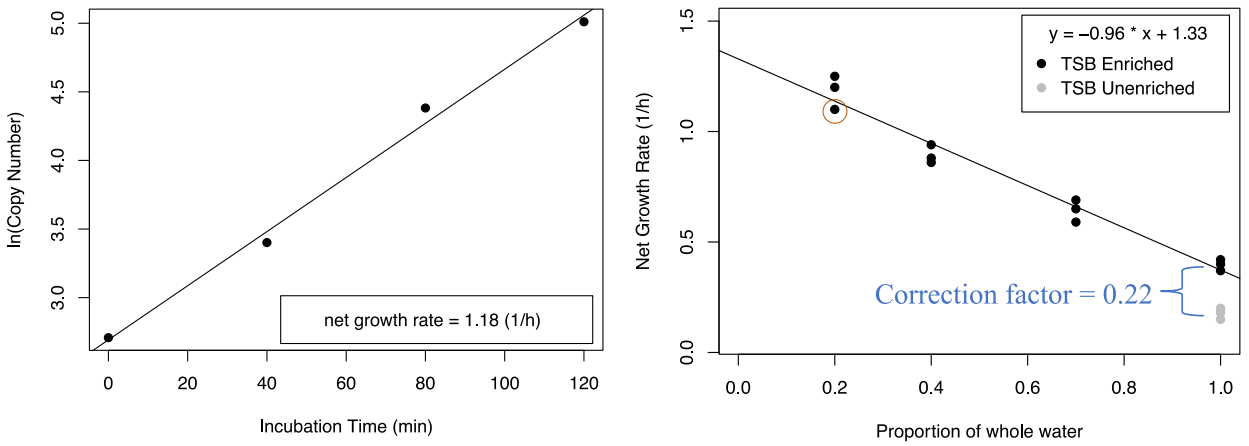

Figure 2.2 Idealized dilution experiment curve based on Landry and Hassett (1982) and Landry et al. (1995) using mock data. Population abundance is tracked over time for each dilution treatment (left panel) in triplicate. The resulting growth rates are plotted against the proportion of whole water to generate the dilution curve (right panel). The singular growth rate generated from the left panel is circled in red on the right panel. The mortality rate is interpreted as negative the slope of the curve (0.96 h^{-1}). The gross growth rate is interpreted as the intercept of the curve (the theoretical full dilution where predation pressure would effectively be zero) corrected by the difference between the growth rates of the enriched and unenriched whole water treatments. Gross growth rate = intercept – correction factor = 1.33 – 0.22 = 1.11 h^{-1}. In this case, enrichment is with tryptic soy broth (TSB).

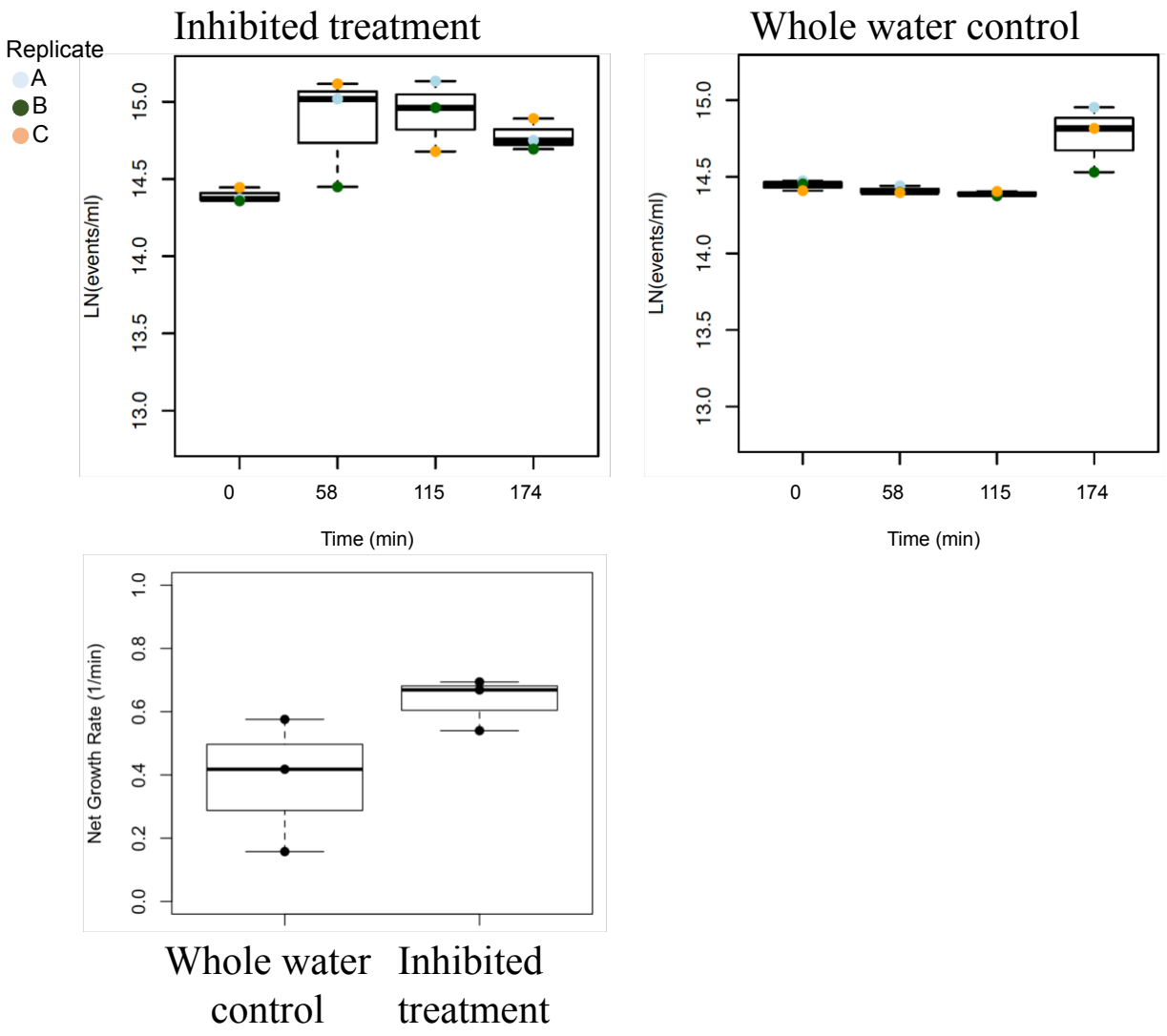

Figure 2.3 Growth rates of total prokaryotes in whole water untreated and with cytochalasin B eukaryotic inhibitor. Values are shown as points in addition to the mean as a bar and standard error around the mean. Gross growth is interpreted as the growth rate in the inhibited treatment (0.384 min^{-1}). Mortality rate is interpreted as the difference in growth rate between the inhibited and whole water treatment (0.634 – 0.384 = 0.250 min^{-1}). There was no significant difference between the growth rates of the control and treatment (t-test, p = 0.245).

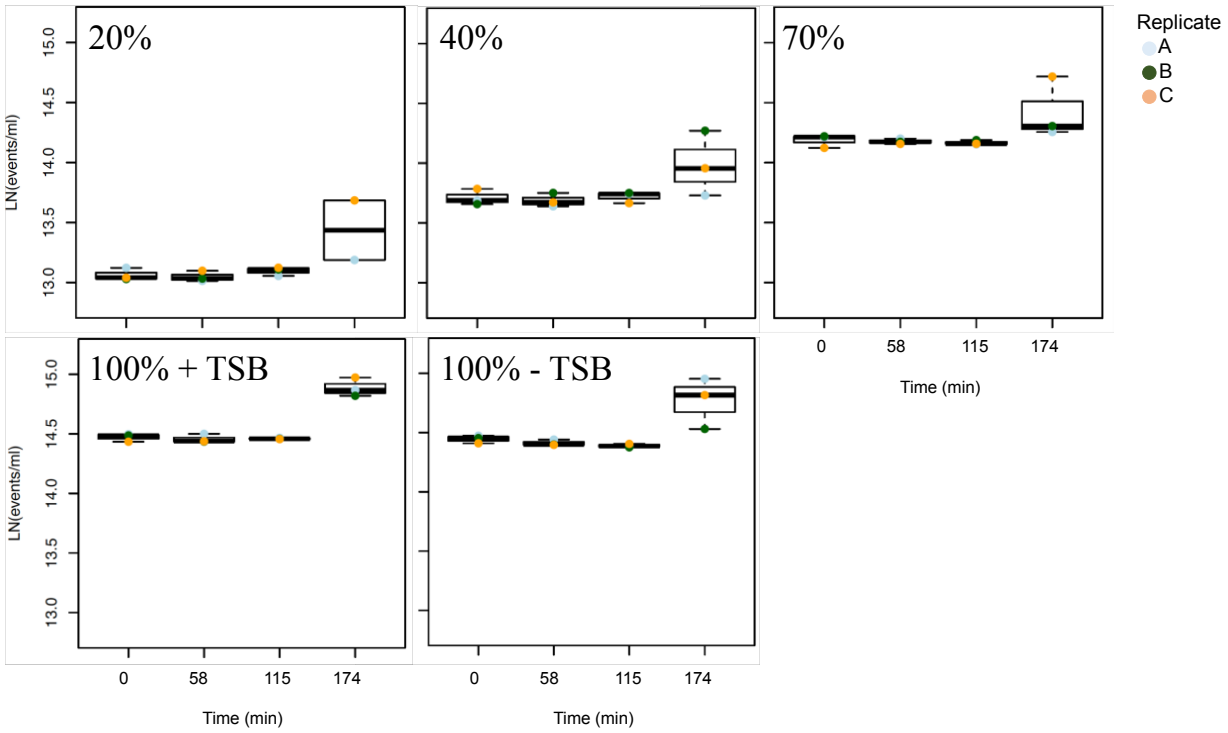

Figure 2.4 Growth curves of total prokaryotes for each treatment in the grazing only dilution experiment (0.2 µm diluent). 100% corresponds to the whole water, undiluted treatment. Counts are expressed in events mL^{-1} which is equivalent to cells mL^{-1}.

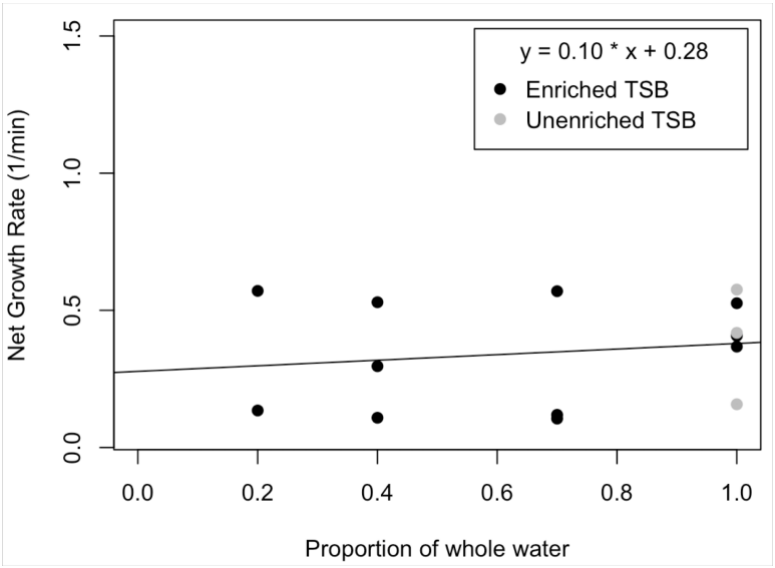

Figure 2.5 Dilution curve for total prokaryote growth rates from the grazing only dilution experiment (see Figure 2.4). Gross growth rate is 0.28 min^{-1} and mortality rate is -0.10 min^{-1}.

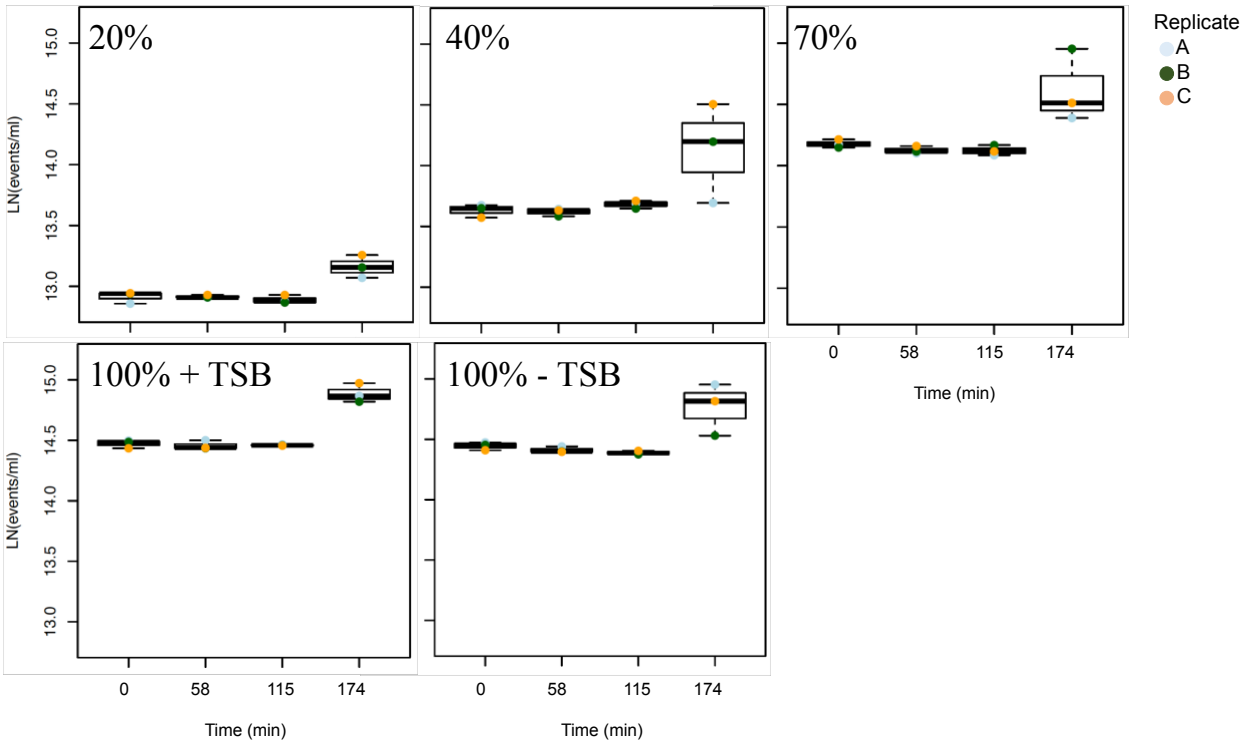

Figure 2.6 Growth curves of total prokaryotes for each treatment in the grazing plus viral lysis dilution experiment (100 kDa diluent). 100% corresponds to the whole water, undiluted treatment. Counts are expressed in events mL^{-1} which is equivalent to cells mL^{-1}.

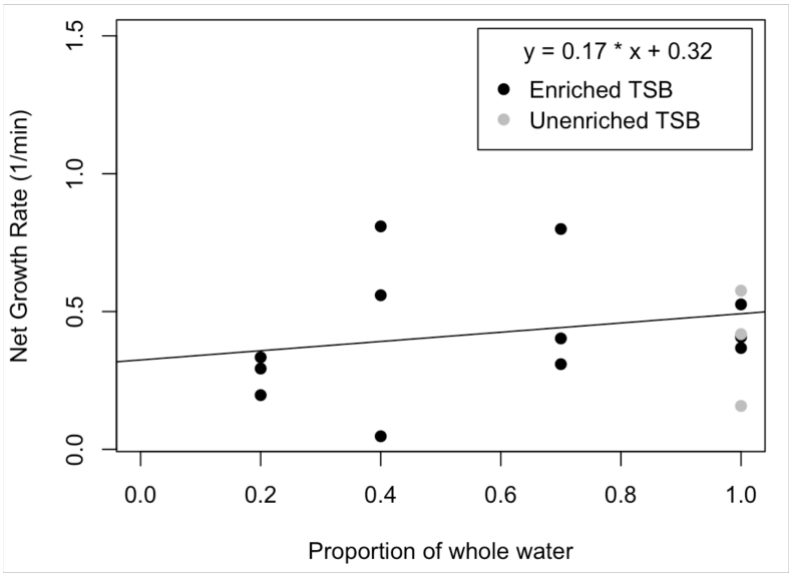

Figure 2.7 Dilution curve for total prokaryote growth rates from the grazing plus viral lysis dilution experiment (see Figure 2.6). Gross growth rate is 0.32 min^{-1} and mortality rate is -0.17 min^{-1}.

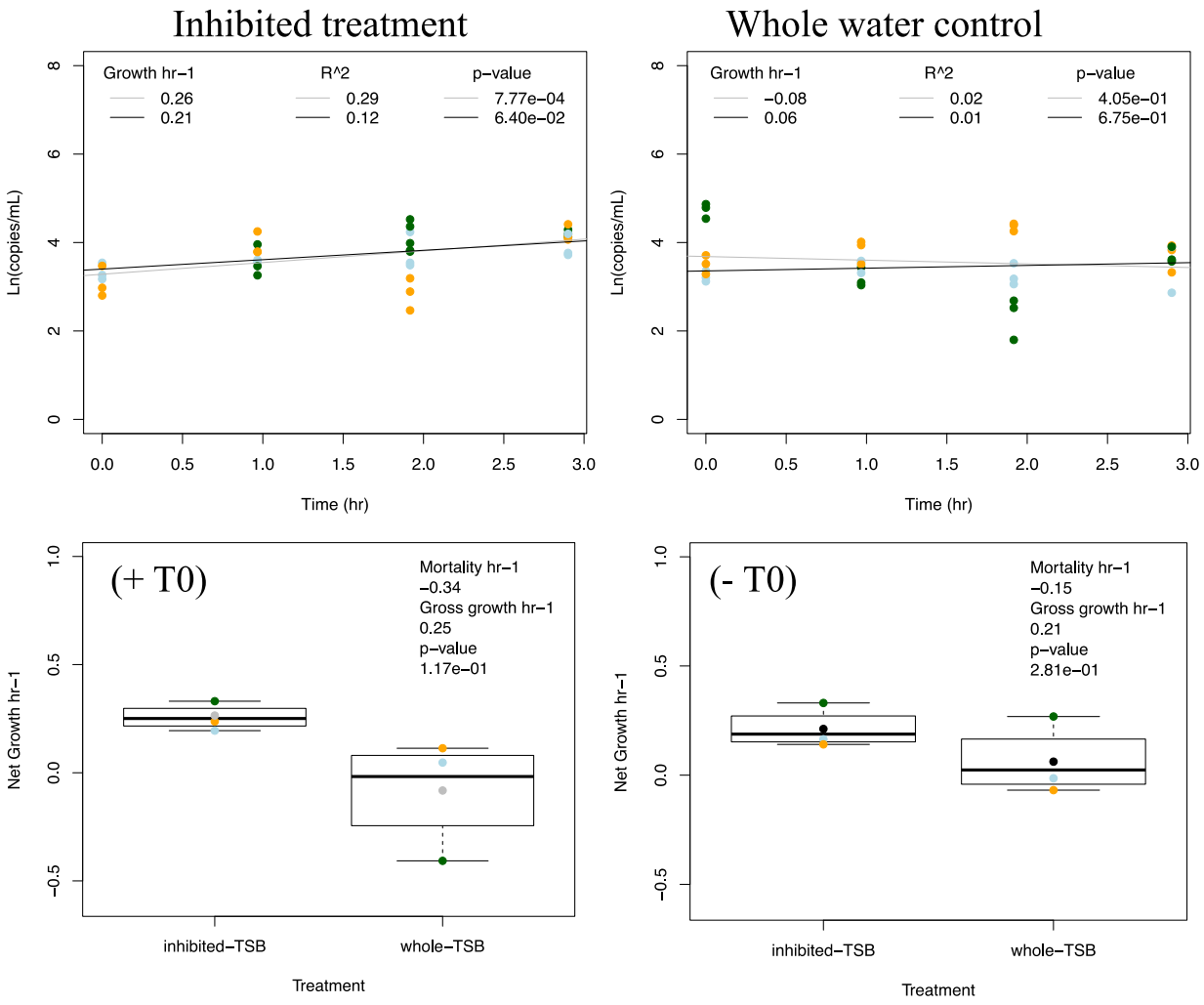

Figure 2.8 Growth rates of *V. vulnificus* in whole water untreated and with cytochalasin B eukaryotic inhibitor. Counts are expressed in copies mL^{-1} which is *vvhA* gene copies mL^{-1}. Linear regression analysis was performed with the initial time point (T0) included (grey line) and without the initial time point to account for a lag in growth (black line). There was not statistically significant growth in the whole water control ($p > 0.05$).

The two bottom panels are comparing the growth rates between the treatments where the bottom left panel includes T0 in calculations and the bottom right panel does not include T0. Gross growth is interpreted as the growth rate in the inhibited treatment (0.25 h^{-1} including T0; 0.21 h^{-1} without T0). Mortality rate is interpreted as the difference in growth rate between the inhibited and whole water treatment (0.34 h^{-1} including T0; 0.15 h^{-1} without T0). There was no significant difference between the growth rates of the control and treatment (t-test, $p = 0.117$ including T0; $p = 0.281$ without T0).

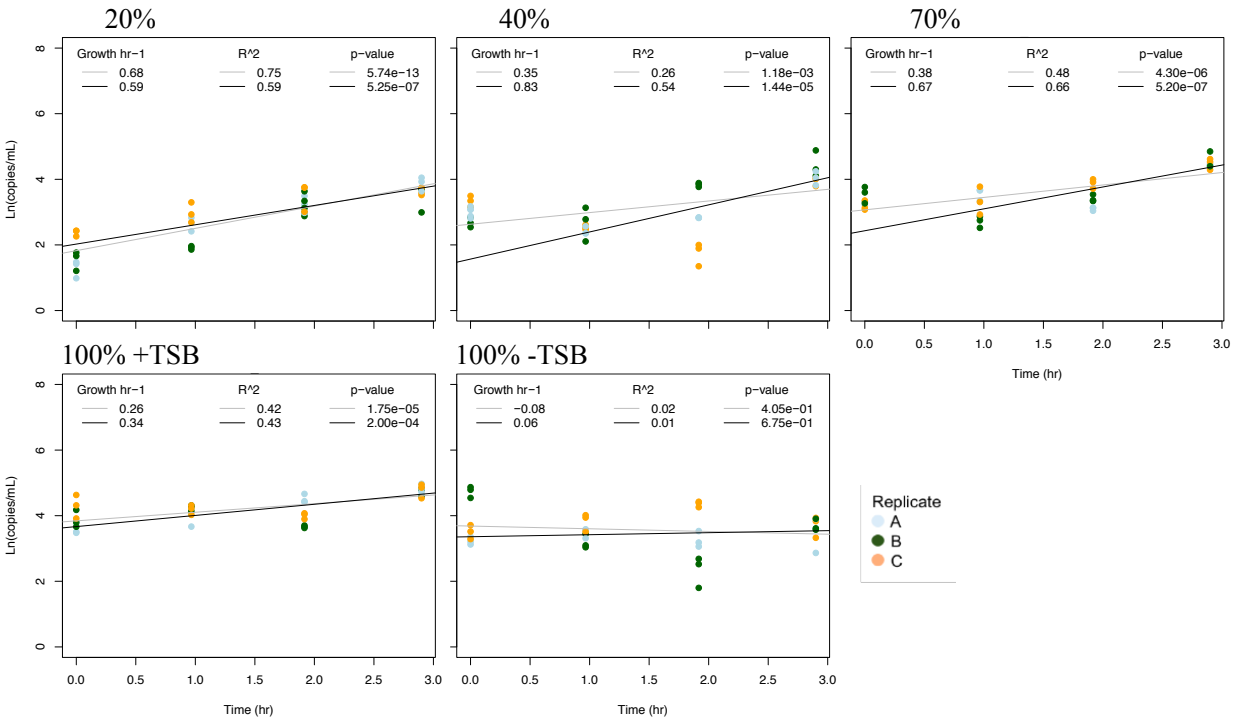

Figure 2.9 Growth rates of *V. vulnificus* from the grazing only dilution experiment (0.2 µm diluent). 100% corresponds to the whole water, undiluted treatment. Counts are expressed in copies mL^{-1} which is *vvhA* gene copies mL^{-1}. Linear regression analysis was performed with the initial time point (T0) included (grey line) and without the initial time point to account for a lag in growth (black line). As intended, there was statistically significant growth in all treatments ($p < 0.05$) except for the whole water without enrichment.

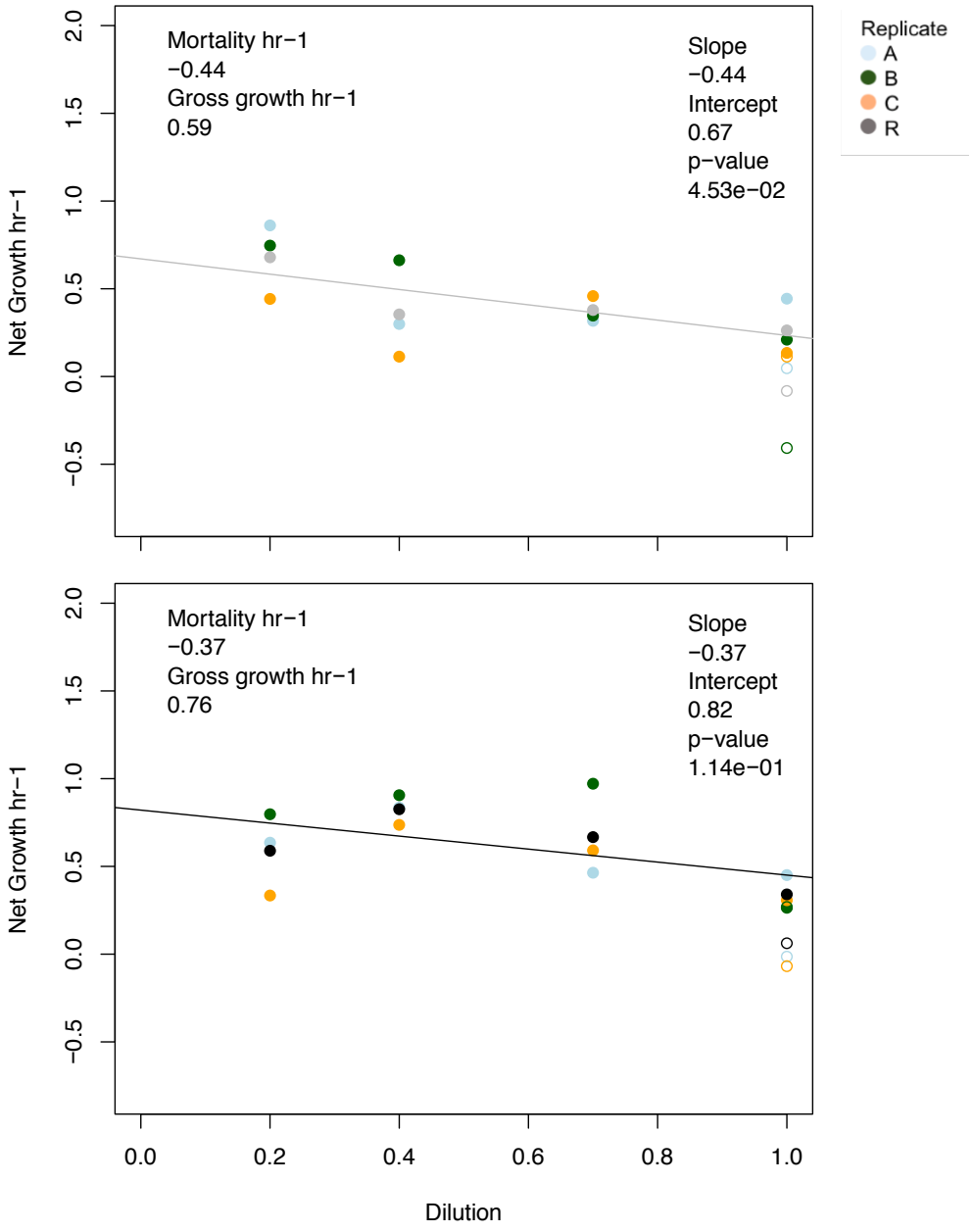

Figure 2.10 Dilution curves for *V. vulnificus* growth rates from the grazing only dilution experiment (see Figure 2.9). Linear regression analysis was performed with the initial time point (T0) included in growth rate calculations for the top panel (grey line) and without the initial time point for the bottom panel (black line). Replicate R is the average growth rate across all the replicates (A, B, C) of a particular treatment. The dilution curve regression is evaluated with replicate R. The average of the whole water without TSB replicates (open circles) is the correction factor which is subtracted from the intercept to calculate the gross growth rate. Gross growth rates were 0.59 h^{-1} including T0 and 0.76 h^{-1} without T0. Mortality rate rates were 0.44 h^{-1} including T0 and 0.37 h^{-1} without T0. There was no significant effect of dilution ($p = 0.05$ including T0; $p = 0.11$ without T0).

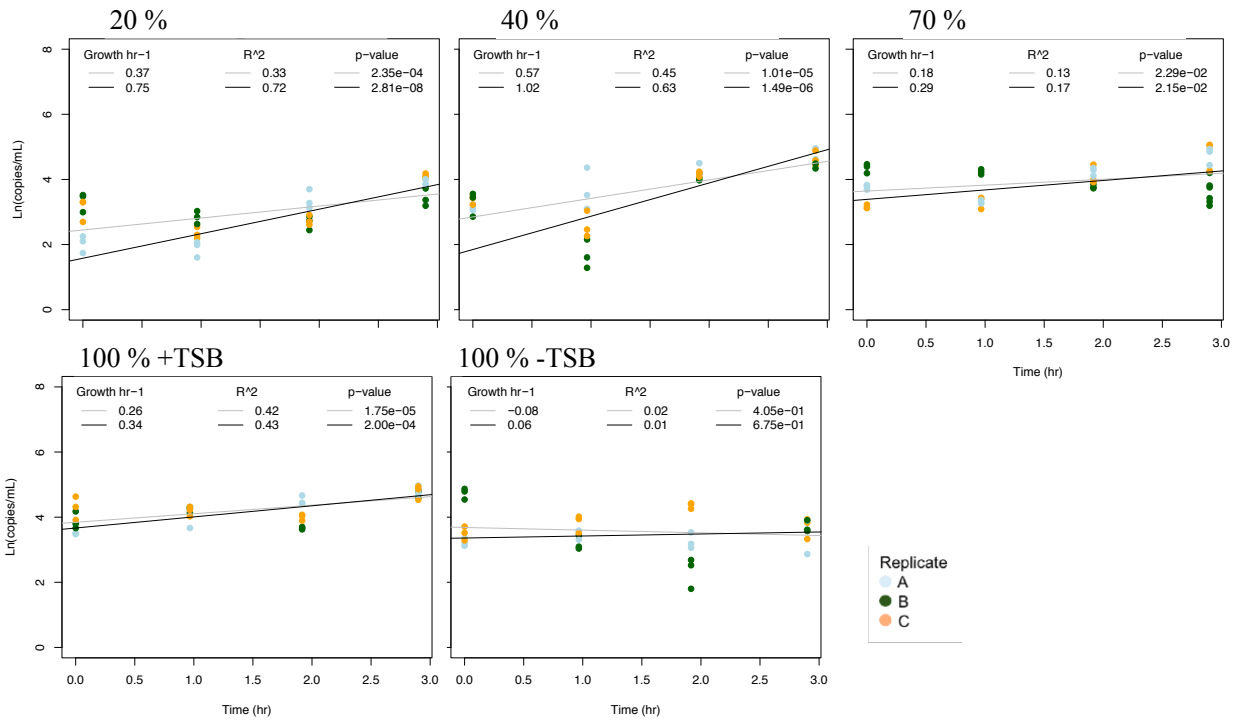

Figure 2.11 Growth rates of *V. vulnificus* from the grazing plus viral lysis dilution experiment (100 kDa diluent). 100% corresponds to the whole water, undiluted treatment. Counts are expressed in copies mL^{-1} which is *vvhA* gene copies mL^{-1}. Linear regression analysis was performed with the initial time point (T0) included (grey line) and without the initial time point to account for a lag in growth (black line). As intended, there was significant growth in all treatments ($p < 0.05$) except for the whole water without enrichment.

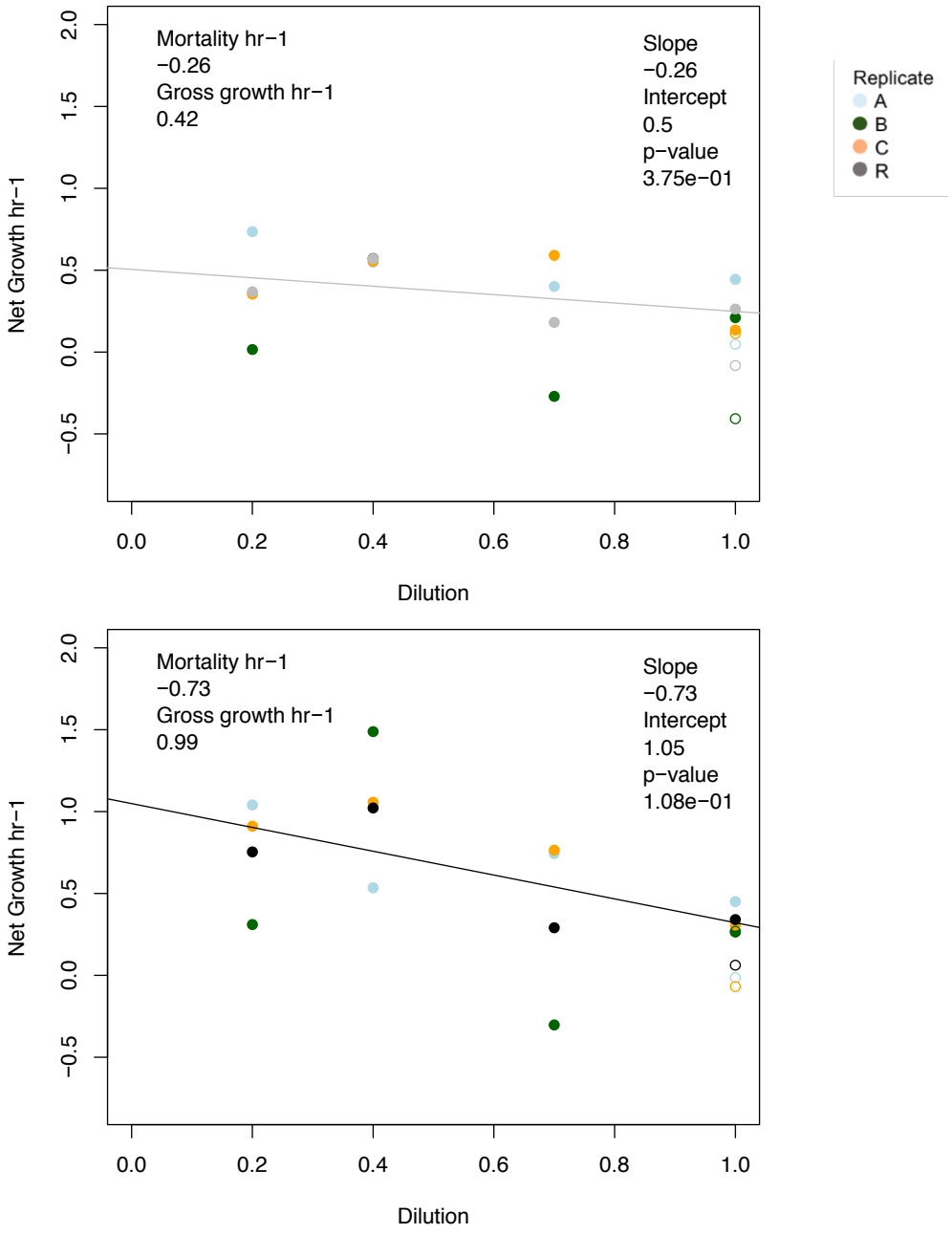

Figure 2.12 Dilution curves for *V. vulnificus* growth rates from the grazing and viral lysis dilution experiment (see Figure 2.11). Linear regression analysis was performed with the initial time point (T0) included in growth rate calculations for the top panel (grey line) and without the initial time point for the bottom panel (black line). Replicate R is the average growth rate across all the replicates (A, B, C) of a particular treatment. The dilution curve regression is evaluated with replicate R. The average of the whole water without TSB replicates (open circles) is the correction factor which is subtracted from the intercept to calculate the gross growth rate. Gross growth rates were 0.42 h^{-1} including T0 and 0.99 h^{-1} without T0. Mortality rate rates were 0.26 h^{-1} including T0 and 0.73 h^{-1} without T0. There was no significant effect of dilution ($p = 0.38$ including T0; $p = 0.11$ without T0).

2.8 ACKNOWLEDGEMENTS

I thank Grieg Steward for his assistance with designing and running the experiments and interpreting the data. I thank Brian Powell for attempting to make meaningful results from the data. I thank the interns and volunteers who assisted with collection of samples from the canal and running the experiments: Shaun Wriston, Han Quach, and Brenna Carroll. This project was funded by NOAA Sea Grant.

2.9 LITERATURE CITED

Bustin, S. A., Benes, V., Garson, J. A., Hellemans, J., Huggett, J., Kubista, M., Mueller, R., Nolan, T., Pfaffl, M. W., Shipley, G. L., Vandesompele, J., & Wittwer, C. T. (2009). The MIQE Guidelines: Minimum Information for Publication of Quantitative Real-Time PCR Experiments. *Clinical Chemistry*, *55*(4), 611–622. https://doi.org/10.1373/clinchem.2008.112797

Campbell, M. S., & Wright, A. C. (2003). Real-Time PCR Analysis of *Vibrio vulnificus* from Oysters. *Applied and Environmental Microbiology*, *69*(12), 7137–7144. https://doi.org/10.1128/AEM.69.12.7137-7144.2003

Chen, C. Y., Wu, K. M., Chang, Y. C., Chang, C. H., Tsai, H. C., Liao, T. L., Liu, Y. M., Chen, H. J., Shen, A. B. T., Li, J. C., Su, T. L., Shao, C. P., Lee, C. T., & Tsai, S. F. (2003). Comparative genome analysis of *Vibrio vulnificus*, a marine pathogen. *Genome Research*, *13*(12), 2577–2587. https://doi.org/10.1101/gr.1295503

Chen, H., Athar, R., Zheng, G., & Williams, H. N. (2011). Prey bacteria shape the community structure of their predators. *The ISME journal*, *5*(8), 1314-1322. https://doi.org/10.1038/ismej.2011.4

Holland, P. M., Abramson, R. D., Watson, R., & Gelfand, D. H. (1991). Detection of specific polymerase chain reaction product by utilizing the 5′ → 3′ exonuclease activity of *Thermus aquaticus* DNA polymerase. *Proceedings of the National Academy of Sciences of the United States of America*, *88*(16), 7276–7280. https://doi.org/10.1073/pnas.88.16.7276

Huehn, S., Eichhorn, C., Urmersbach, S., Breidenbach, J., Bechlars, S., Bier, N., Alter, T., Bartelt, E., Frank, C., Oberheitmann, B., Gunzer, F., Brennholt, N., Böer, S., Appel, B., Dieckmann, R., & Strauch, E. (2014). Pathogenic vibrios in environmental, seafood and clinical sources in Germany. *International Journal of Medical Microbiology*, *304*(7), 843-850. https://doi.org/10.1016/j.ijmm.2014.07.010

Jacquet, S., Domaizon, I., Personnic, S., Ram, A. S. P., Hedal, M., Duhamel, S., & Sime-Ngando, T. (2005). Estimates of protozoan-and viral-mediated mortality of bacterioplankton in Lake Bourget (France). *Freshwater Biology*, *50*(4), 627-645. https://doi.org/10.1111/j.1365-2427.2005.01349.x

Jones, M. K., & Oliver, J. D. (2009). *Vibrio vulnificus*: Disease and pathogenesis. *Infection and Immunity*, *77*(5), 1723-1733. https://doi.org/10.1128/IAI.01046-08

Kaspar, C. W., & Tamplin, M. L. (1993). Effects of temperature and salinity on the survival of *Vibrio vulnificus* in seawater and shellfish. *Applied and Environmental Microbiology*, *59*(8), 2425–2429. https://doi.org/10.1128/aem.59.8.2425-2429.1993

Kelly, L. W., Nelson, C. E., Haas, A. F., Naliboff, D. S., Calhoun, S., Carlson, C. A., Edwards, R. A., Fox, M. D., Hatay, M., Johnson, M. D. and Kelly, E. L. (2019). Diel population and functional synchrony of microbial communities on coral reefs. *Nature*

Communications, *10*(1), 1-9. https://doi.org/10.1038/s41467-019-09419-z

Kimmance, S. A., Wilson, W. H., & Archer, S. D. (2007). Modified dilution technique to estimate viral versus grazing mortality of phytoplankton: limitations associated with method sensitivity in natural waters. *Aquatic Microbial Ecology*, *49*(3), 207-222. https://doi.org/10.3354/ame01136

Landry, M. R., & Hassett, R. (1982). Estimating the grazing impact of marine micro-zooplankton. *Marine Biology*, 67(3), 283-288. https://doi.org/10.1007/BF00397668

Landry, M. R., Kirshtein, J., & Constantinou, J. (1995). A refined dilution technique for measuring the community grazing impact of microzooplankton, with experimental tests in the central equatorial Pacific. *Marine Ecology Progress Series*, *120*(1), 53-63. https://doi.org/10.3354/meps120053

Li, Q. P., Franks, P. J., & Landry, M. R. (2017). Recovering growth and grazing rates from nonlinear dilution experiments. *Limnology and Oceanography*, *62*(5), 1825-1835. https://doi.org/10.1002/lno.10536

Mojica, K. D., Huisman, J., Wilhelm, S. W., & Brussaard, C. P. (2016). Latitudinal variation in virus-induced mortality of phytoplankton across the North Atlantic Ocean. *The ISME journal*, *10*(2), 500-513. https://doi.org/10.1038/ismej.2015.130

Motes, M. L., DePaola, A., Cook, D. W., Veazey, J. E., Hunsucker, J. C., Garthright, W. E., Blodgett, R. J., & Chirtel, S. J. (1998). Influence of water temperature and salinity on *Vibrio vulnificus* in Northern Gulf and Atlantic Coast oysters (*Crassostrea virginica*). *Applied and Environmental Microbiology*, *64*(4), 1459–1465. https://doi.org/10.1128/aem.64.4.1459-1465.1998

Nelson, C. E., Donahue, M. J., Dulaiova, H., Goldberg, S. J., La Valle, F. F., Lubarsky, K., Miyano, J., Richardson, C., Silbiger, N. J., & Thomas, F. I. M. (2015). Fluorescent dissolved organic matter as a multivariate biogeochemical tracer of submarine groundwater discharge in coral reef ecosystems. *Marine Chemistry*, *177*, 232–243. https://doi.org/10.1016/j.marchem.2015.06.026

Nigro, O. D. (2012). Environmental controls on *Vibrio vulnificus* and other pathogenic vibrios in tropical and subtropical coastal waters. *ProQuest Dissertations Publishing*. Retrieved from https://scholarspace.manoa.hawaii.edu/handle/10125/101007

Nigro, O. D., & Steward, G. F. (2015). Differential specificity of selective culture media for enumeration of pathogenic vibrios: Advantages and limitations of multi-plating methods. *Journal of Microbiological Methods*, *111*, 24–30. https://doi.org/10.1016/j.mimet.2015.01.014

Nigro, O. D., Culley, A. I., & Steward, G. F. (2012). Complete genome sequence of bacteriophage VvAW1, which infects Vibrio vulnificus. *Standards in genomic sciences*, *6*(3), 415-420. https://doi.org/10.4056/sigs.2846206

Nuss, E. (2016). Predicting pathogenic bacteria concentrations with a coupled microbial-physical model. *ProQuest Dissertations Publishing*. Retrieved from https://www.soest.hawaii.edu/oceanography/masters/2016-Nuss.pdf

Ottesen, E. A., Young, C. R., Gifford, S. M., Eppley, J. M., Marin, R., Schuster, S. C., Scholin, C. A. and DeLong, E. F. (2014). Multispecies diel transcriptional oscillations in open ocean heterotrophic bacterial assemblages. *Science*, *345*(6193), 207-212. https://doi.org/10.1126/science.1252476

Pfaffl, M. W. (2001). A new mathematical model for relative quantification in real-time RT–PCR. *Nucleic Acids Research*, *29*(9), E45. https://doi.org/10.1093/nar/29.9.e45

R Core Team (2019). R: A language and environment for statistical computing. R Foundation for Statistical Computing, Vienna, Austria. URL https://www.R-project.org/

Randa, M. A., Polz, M. F., & Lim, E. (2004). Effects of temperature and salinity on *Vibrio vulnificus* population dynamics as assessed by quantitative PCR. *Applied and Environmental Microbiology*, *70*(9), 5469–5476. https://doi.org/10.1128/AEM.70.9.5469-5476.2004

Tijdens, M., Van de Waal, D. B., Slovackova, H., Hoogveld, H. L., & Gons, H. J. (2008). Estimates of bacterial and phytoplankton mortality caused by viral lysis and microzooplankton grazing in a shallow eutrophic lake. *Freshwater Biology*, *53*(6), 1126-1141. https://doi.org/10.1111/j.1365-2427.2008.01958.x

Worden, A. Z., & Binder, B. J. (2003). Application of dilution experiments for measuring growth and mortality rates among *Prochlorococcus* and *Synechococcus* populations in oligotrophic environments. *Aquatic Microbial Ecology*, *30*(2), 159-174. https://doi.org/10.3354/ame030159

Worden, A. Z., Seidel, M., Smriga, S., Wick, A., Malfatti, F., Bartlett, D., & Azam, F. (2006). Trophic regulation of *Vibrio cholerae* in coastal marine waters. *Environmental Microbiology*, *8*(1), 21-29. https://doi.org/10.1111/j.1462-2920.2005.00863.x